

A ternary mixture model with dynamic boundary conditions

Shuang Liu,¹ Yue Wu,² and Xueping Zhao ^{a2}

¹*Department of Mathematics, University of North Texas,
1155 Union Circle, Denton, Texas 76203-5017, USA*

²*Department of Mathematical Sciences,
University of Nottingham Ningbo China,
Taikang East Road 199, 315100 Ningbo, China*

Abstract

The influence of short-range interactions between a multi-phase, multi-component mixture and a solid wall in confined geometries is crucial in life sciences and engineering. In this work, we extend the Cahn-Hilliard model with dynamic boundary conditions from a binary to a ternary mixture, employing the Onsager principle that accounts for cross-coupling between forces and fluxes in both bulk and surface. Moreover, we have developed a linear, second-order, and unconditionally energy stable numerical scheme for solving the governing equations, utilizing the Invariant Energy Quadratization (IEQ) method. This efficient solver allows us to explore the impacts of wall-mixture interactions and dynamic boundary conditions on phenomena like spontaneous phase separation, coarsening processes, and the wettability of droplets on surfaces. We observe that wall-mixture interactions influence not only surface phenomena, such as droplet contact angles, but also patterns deep within the bulk. Additionally, the relaxation rates control the droplet spreading on surfaces. Furthermore, the cross-coupling relaxation rates in the bulk significantly affect coarsening patterns. Our work establishes a comprehensive framework for studying multi-component mixtures in confined geometries.

^a Corresponding author: Xueping.Zhao@nottingham.edu.cn

1. INTRODUCTION

The physics of multi-component mixtures, including spontaneous phase separation, nucleation and growth, and coarsening have been well-studied both theoretically and experimentally. The question of how the multi-component multi-phase system interacts with solid walls in confined geometries has gained much attention due to its wide applications in life science and engineering, e.g. membrane-less organelles formation and wetting on the membrane-bound organelles in living cells [1, 6, 20]; micro-fluid close to a solid interface in microfluidic devices [45]; thin films of polymer blends in a slab geometry [7, 29, 42], and so on.

Numerous methods have been developed to study interface problems and their interaction with solid walls. For instance, the lattice Boltzmann model has garnered considerable attention for simulating multi-phase and multi-component systems with complex boundary conditions, as demonstrated by several studies [23, 39, 40, 43, 44]. Additionally, the exploration of wetting properties in ternary mixture models has been a significant focus [38, 49, 50]. For example, Liang et al. [32] formulated a wetting boundary condition for ternary fluids interacting with a solid substrate, applying this to the lattice Boltzmann model. The Volume Of Fluid (VOF) technique is particularly effective in scenarios involving solid obstacles, as it integrates the contact angle by applying appropriate boundary conditions to the fluid-function's gradient at solid interfaces. Therefore, VOF has been extensively used in fluid dynamics analyses within complex porous structures [14–16, 30, 31]. However, among all these methods, the phase field method stands out as the most effective tool for modeling and simulating multi-phase systems. Its inherent flexibility in handling complex topological changes in the phases, coupled with its ability to seamlessly integrate with various boundary conditions, makes it a superior choice for addressing the complexities of interface problems in multi-component systems.

Cahn–Hilliard equation is a fundamental phase field model. Since it is firstly proposed in materials science to describe the pattern formation evolution of microstructures during the phase separation process in binary alloys [9, 11], the Cahn–Hilliard equation and its variants have been successfully applied in a wide variety of segregation-like phenomena in science, see for instance [4, 17, 18, 22, 24, 28, 33, 36] and the references therein. In this study, we denote the domain as Ω , the boundary of the domain Γ . We introduce ϕ , which represents the volume fraction of a specific component within the mixture. $\phi \in (0, 1)$ is dimensionless and quantifies the proportion of the total volume occupied by a given component, providing insight into the concentration and

distribution of that component within the system. The total free energy of the system reads

$$F = \int_{\Omega} \left[f_b(\phi) + \frac{\kappa}{2} |\nabla\phi|^2 \right] d\mathbf{x}, \quad (1)$$

where $f_b(\phi)$ is the bulk free energy density function, the term $\frac{\kappa}{2} |\nabla\phi|^2$ represents the interface energy between phases. The Cahn–Hilliard equation has the following format:

$$\partial_t\phi = \nabla M \cdot \nabla\mu, \quad (2)$$

where mobility M can be either a constant or concentration-dependent function, and μ is the chemical potential of the component ϕ . The boundary conditions include the following two categories:

1. periodic boundary conditions.
2. physical boundary conditions. e.g. homogeneous Neumann boundary conditions.

However, in some systems, e.g. phase separation in confined geometries, the condensate will interact with boundaries, and thus more generic boundary conditions, which describe the interaction between wall and condensates, are introduced. In this work, we will focus on the study of generic boundary conditions.

The influence of boundaries (solid walls) on the phase separation process of binary mixtures has attracted lots of attention from scientists. For instance, W. Dieterich, etc. [17] introduced the dynamic boundary conditions in 1997:

$$\partial_n\mu|_{\Gamma} = 0, \quad (3a)$$

$$\partial_t\phi|_{\Gamma} = -\Gamma_s \left[\kappa \partial_n\phi + f_s' - \kappa_{\Gamma} \Delta_{\Gamma}\phi_{\Gamma} \right], \quad (3b)$$

where f_s is the surface free energy density which represents the short-range interaction between mixture components and the solid wall, Δ_{Γ} stands for the Laplace–Beltrami operator on the boundary surface Γ , and Γ_s defines a surface kinetic coefficient and the term $\kappa \partial_n\phi$ is due to the surface contribution that comes from the variation of the bulk free energy f_b . The boundary (3a) is simply the condition that no current can flow through the surface, while the boundary (3b) can be derived by requiring the system to tend to minimize its surface free energy,

$$F_s = \int_{\Omega} \left[\frac{\kappa_{\Gamma}}{2} |\nabla_{\Gamma}\phi_{\Gamma}|^2 + f_s \right]. \quad (4)$$

Boundary conditions of similar form as Eqs. (3) have also been derived from a semi-infinite Ising model with Kawasaki spin exchange dynamics [5, 37]. In 2011, Goldstein, etc. derived a Cahn–Hilliard model in a domain with non-permeable walls[22]. In this model, they assumed that the

total mass in the bulk and on the boundary, i.e.

$$\int_{\Omega} \phi(\mathbf{x}) d\mathbf{x} + \int_{\Gamma} \phi(\mathbf{x}) dS, \quad (5)$$

is conserved. Its boundary conditions read

$$\partial_t \phi|_{\Gamma} = \nabla_{\Gamma} M \cdot \nabla_{\Gamma} \mu_{\Gamma} - \beta M \partial_n \mu, \quad (6a)$$

$$\mu|_{\Gamma} = \beta \left[\kappa \partial_n \phi + f_s' - \kappa_{\Gamma} \Delta_{\Gamma} \phi_{\Gamma} \right]. \quad (6b)$$

In addition, they proved the existence and uniqueness of weak solutions and studied their asymptotic behavior as time goes to infinity.

Liu Chun and Wu Hao [33] introduced a Liu-Wu model in 2019 with non-flux boundary conditions for chemical potential and Cahn–Hilliard type gradient flow on the boundary, i.e.

$$\partial_n \mu = 0, \quad (7a)$$

$$\partial_t \phi|_{\Gamma} = \nabla_{\Gamma} M \cdot \nabla_{\Gamma} \left[\kappa \partial_n \phi + f_s' - \kappa_{\Gamma} \Delta_{\Gamma} \phi_{\Gamma} \right]. \quad (7b)$$

In 2021, Patrik Knopf and collaborators proposed a general model[36]: KLLM model.

$$L \partial_n \mu = -\mu|_{\Gamma} + \beta \left[\kappa \partial_n \phi + f_s' - \kappa_{\Gamma} \Delta_{\Gamma} \phi_{\Gamma} \right], \quad (8a)$$

$$\partial_t \phi|_{\Gamma} = \nabla_{\Gamma} M \cdot \nabla_{\Gamma} \left[\kappa \partial_n \phi + f_s' - \kappa_{\Gamma} \Delta_{\Gamma} \phi_{\Gamma} \right] - \beta M \partial_n \mu. \quad (8b)$$

Harald Garcke etc [21] did the nonlinear analysis, long-time dynamics of the Cahn–Hilliard equation with kinetic rate dependent dynamic boundary conditions for the KLLM model. We refer to [46] for reviews of the model and analysis.

Correspondingly, there are numerical studies for binary mixture models with dynamic boundary conditions. For example, W. Dieterich etc. proposed an implicit numerical scheme [28] to solve the Cahn–Hilliard equation with (3). The authors discretized the solution in space using the finite difference method on edge points. Stability analysis was derived and a variable time-stepping strategy was employed to simulate the system for a long time. Furthermore, the numerical scheme is conditionally gradient stable, which means that the free energy decreases monotonously in time. In 2017, Shuji Yoshikawa and collaborators [19] constructed a structure-preserving finite difference scheme for the Cahn–Hilliard equation with dynamic boundary conditions in the one-dimensional case for Goldstein model (6). Unlike the space discretization in [28], the author used the finite difference method on center points. The existence of the solution and the error estimate were also obtained. In addition, the laws of mass conservation and energy dissipation were satisfied in the

discrete level. Zhang Zhengru and collaborators developed a second order stabilized semi-implicit scheme [47] for Liu-Wu model (7). The corresponding energy stability and convergence analysis of the scheme were derived theoretically.

Besides the binary mixture models, phase field models for ternary mixture systems have been developed due to their frequent real-world applications, as indicated in studies [2, 3, 26]. Wetting behavior [25, 48] has also been proposed based on the phase field models. For example, a phase field model for multi-component Cahn-Hilliard systems in complex domains was developed in [48], considering contact angle or no mass flow boundary conditions. Building on this, [25] extended the geometrical formulation of wetting conditions using weighted contact angles defined within the implementation of wetting conditions, following the concept of the diffusive interface [8]. This innovative phase field model efficiently describes the dynamic behavior of compound droplets in contact with solid objects.

However, we note that dynamic boundary conditions are missing in the aforementioned multi-component phase field models. Moreover, to the best of our knowledge, a ternary mixture model with the force-flux cross-coupling relations has not been explored yet. In summary, based on the above discussion, we focus on the following aims in this work:

1. Derive a model for a ternary mixture with the force-flux cross-coupling relations in a confined geometry with dynamic boundary conditions based on the Onsager principle and irreversible thermodynamics [13, 27, 34, 35, 41, 52].
2. Develop a linear second-order unconditionally energy stable numerical scheme for the derived model based on the Invariant Energy Quadraticization(IEQ) method [51, 53–55].
3. Investigate equilibrium and out of equilibrium properties of the system based on the numerical simulations.

Section 2 details the derivation of a kinetic model. This model, which addresses a ternary mixture within confined geometries and its interaction with adjacent solid walls, is formulated using principles of irreversible thermodynamics. It features conservation of total mass and a decrease in total energy over time. The mathematical model undergoes an equivalent reformulation based on the IEQ method in Section 3, where we also introduce a second-order, linear, unconditional energy stable numerical scheme for the revised model. Section 4 examines how spontaneous phase separation and surface wettability are influenced by various model parameters using numerical studies. The paper concludes in Section 5, where we summarize our findings.

2. MATHEMATICAL MODEL DERIVATION

In this section, we will extend the binary mixture model with dynamic boundary conditions to a ternary mixture model, based on the Onsager principles[13, 34, 35, 41, 52]. We denote the volume fractions of three components as ϕ_1 , ϕ_2 , and ϕ_3 , where $\phi_3 = 1 - \phi_1 - \phi_2$ based on the incompressibility assumption. The total free energy of the system includes two contributions: one is the free energy in the bulk Ω , and another on the surface Γ , i.e.

$$E = E_{\text{bulk}} + E_{\text{surf}}, \quad (9)$$

where the bulk free energy E_{bulk} and surface free energy E_{surface} read

$$E_{\text{bulk}} = \int_{\Omega} \left[f_b(\phi_1, \phi_2) + \frac{\kappa_1}{2} |\nabla \phi_1|^2 + \frac{\kappa_2}{2} |\nabla \phi_2|^2 + \kappa_{12} \nabla \phi_1 \cdot \nabla \phi_2 \right], \quad (10)$$

$$E_{\text{surf}} = \int_{\Gamma} \left[f_s(\phi_{1\Gamma}, \phi_{2\Gamma}) + \frac{\kappa_{1\Gamma}}{2} |\nabla_{\Gamma} \phi_{1\Gamma}|^2 + \frac{\kappa_{2\Gamma}}{2} |\nabla_{\Gamma} \phi_{2\Gamma}|^2 + \kappa_{12\Gamma} \nabla_{\Gamma} \phi_{1\Gamma} \cdot \nabla_{\Gamma} \phi_{2\Gamma} \right]. \quad (11)$$

κ_i , $\kappa_{i\Gamma}$, $i = 1, 2, 12$ are gradient coefficients associated with interface free energies. For simplicity, we set $\kappa_{12} = 0$, and $\kappa_{12\Gamma} = 0$ in the following study. ∇_{Γ} denotes the gradient operator on the surface. The bulk free energy density function $f_b(\phi_1, \phi_2)$ and surface free energy density function $f_s(\phi_{1\Gamma}, \phi_{2\Gamma})$ are defined as Flory-Huggins free energy and a second order polynomial based on application in polymer field [10],

$$f_b(\phi_1, \phi_2) = \frac{k_B T}{\nu} \left[\frac{\phi_1}{n_1} \ln \phi_1 + \frac{\phi_2}{n_2} \ln \phi_2 + (1 - \phi_1 - \phi_2) \ln(1 - \phi_1 - \phi_2) + \chi_{12} \phi_1 \phi_2 \right. \\ \left. + \chi_{13} \phi_1 (1 - \phi_1 - \phi_2) + \chi_{23} \phi_2 (1 - \phi_1 - \phi_2) + \omega_1 \phi_1 + \omega_2 \phi_2 \right], \quad (12)$$

$$f_s(\phi_{1\Gamma}, \phi_{2\Gamma}) = \frac{k_B T}{\nu_s} \left[h_1 \phi_{1\Gamma} + g_1 \phi_{1\Gamma}^2 + h_2 \phi_{2\Gamma} + g_2 \phi_{2\Gamma}^2 + \gamma \phi_{1\Gamma} \phi_{2\Gamma} \right], \quad (13)$$

where $\nu_i = n_i \nu$ represents the molecule volume of component i , $i = 1, 2$, and ν the molecule volume of component 3. For simplicity, we assume the molecule volumes of each component are equivalent, i.e. $\nu_1 = \nu_2 = \nu$ and $n_1 = n_2 = 1$. k_B is the boltzmann constant and T is the temperature of the isotropic system. The term $\chi_{ij} \phi_i \phi_j$ refers to the interaction strength between the component i and the component j . $\omega_i \phi_i$ denotes the internal free energy for component i in the bulk Ω . On the surface, $h_i \phi_i$, $i = 1, 2$ is the linear order term, which denotes the interaction proportional to the component volume fractions. The quadratic $g_i \phi_i^2$ depicts the molecule-molecule interactions of each components near by the wall, while $\gamma \phi_1 \phi_2$ describes the coupling interaction between components on the surface.

We assume that there is no chemical reaction in the system, that is, each component of the mixture conserves the total mass. We write the conservation laws as follows:

$$\partial_t \phi_1 + \nabla \cdot \mathbf{J}_1 = 0, \quad (14)$$

$$\partial_t \phi_2 + \nabla \cdot \mathbf{J}_2 = 0. \quad (15)$$

2.1. Irreversible thermodynamics

We consider a closed system in this work. According to irreversible thermodynamics, the entropy product rate is inversely proportional to the energy change rate.

$$\begin{aligned} -T\partial_t S &= \frac{dE}{dt} = \frac{\partial E}{\partial \phi_1} \frac{\partial \phi_1}{\partial t} + \frac{\partial E}{\partial \phi_2} \frac{\partial \phi_2}{\partial t} + \frac{\partial E}{\partial \phi_{1\Gamma}} \frac{\partial \phi_{1\Gamma}}{\partial t} + \frac{\partial E}{\partial \phi_{2\Gamma}} \frac{\partial \phi_{2\Gamma}}{\partial t} \\ &\quad + \frac{\partial E}{\partial \nabla \phi_1} \frac{\partial \nabla \phi_1}{\partial t} + \frac{\partial E}{\partial \nabla \phi_2} \frac{\partial \nabla \phi_2}{\partial t} + \frac{\partial E}{\partial \nabla_{\Gamma} \phi_{1\Gamma}} \frac{\partial \nabla_{\Gamma} \phi_{1\Gamma}}{\partial t} + \frac{\partial E}{\partial \nabla_{\Gamma} \phi_{2\Gamma}} \frac{\partial \nabla_{\Gamma} \phi_{2\Gamma}}{\partial t} \end{aligned} \quad (16)$$

$$\begin{aligned} &= \int_{\Gamma} dS \left[\mathbf{n} \cdot \kappa_1 \nabla \phi_1 + \left(\frac{\partial f_s}{\partial \phi_{1\Gamma}} - \kappa_{1\Gamma} \Delta_{\Gamma} \phi_1 \right) \right] \frac{\partial \phi_{1\Gamma}}{\partial t} \\ &\quad + \int_{\Gamma} dS \left[\mathbf{n} \cdot \kappa_2 \nabla \phi_2 + \left(\frac{\partial f_s}{\partial \phi_{2\Gamma}} - \kappa_{2\Gamma} \Delta_{\Gamma} \phi_2 \right) \right] \frac{\partial \phi_{2\Gamma}}{\partial t} \\ &\quad - \int_{\Gamma} dS \left[\frac{\mu_1}{\nu_1} \mathbf{n} \cdot \mathbf{J}_1 + \frac{\mu_2}{\nu_2} \mathbf{n} \cdot \mathbf{J}_2 \right] + \int_{\Omega} dx \left[\nabla \frac{\mu_1}{\nu_1} \cdot \mathbf{J}_1 + \nabla \frac{\mu_2}{\nu_2} \cdot \mathbf{J}_2 \right], \end{aligned} \quad (17)$$

where the chemical potentials in the bulk for components 1 and 2 are defined as

$$\mu_1 = \nu_1 \frac{\delta E}{\delta \phi_1} = \nu_1 \left[\frac{\partial f_b}{\partial \phi_1} - \kappa_1 \Delta \phi_1 \right], \quad (18)$$

$$\mu_2 = \nu_2 \frac{\delta E}{\delta \phi_2} = \nu_2 \left[\frac{\partial f_b}{\partial \phi_2} - \kappa_2 \Delta \phi_2 \right]. \quad (19)$$

We achieve the conjugate fluxes and forces as follows:

$$\mathbf{J}_1 \longleftrightarrow -\nabla \mu_1, \quad x \in \Omega, \quad (20a)$$

$$\mathbf{J}_2 \longleftrightarrow -\nabla \mu_2, \quad x \in \Omega, \quad (20b)$$

$$\partial_t \phi_{1\Gamma} \longleftrightarrow - \left(\mathbf{n} \cdot \kappa_1 \nabla \phi_1 + \frac{\partial f_s}{\partial \phi_{1\Gamma}} - \kappa_{1\Gamma} \Delta_{\Gamma} \phi_1 \right), \quad x \in \Gamma, \quad (20c)$$

$$\partial_t \phi_{2\Gamma} \longleftrightarrow - \left(\mathbf{n} \cdot \kappa_2 \nabla \phi_2 + \frac{\partial f_s}{\partial \phi_{2\Gamma}} - \kappa_{2\Gamma} \Delta_{\Gamma} \phi_2 \right), \quad x \in \Gamma, \quad (20d)$$

Based on the Onsager principle, we define a symmetric positive definite mobility function between conjugate fluxes and forces in both the bulk Ω and the surface Γ , i.e.

$$\mathbf{J}_1 = -M_1(\phi_1, \phi_2)\nabla\mu_1 - M_{12}(\phi_1, \phi_2)\nabla\mu_2, \quad (21a)$$

$$\mathbf{J}_2 = -M_{12}(\phi_1, \phi_2)\nabla\mu_1 - M_2(\phi_1, \phi_2)\nabla\mu_2, \quad (21b)$$

$$\partial_t\phi_{1\Gamma} = -\Gamma_1\left[\mathbf{n}\cdot\kappa_1\nabla\phi_1 - \kappa_{1\Gamma}\Delta_\Gamma\phi_{1\Gamma} + \frac{\partial f_s}{\partial\phi_{1\Gamma}}\right] - \Gamma_{12}\left[\mathbf{n}\cdot\kappa_2\nabla\phi_2 - \kappa_{2\Gamma}\Delta_\Gamma\phi_{2\Gamma} + \frac{\partial f_s}{\partial\phi_{2\Gamma}}\right], \quad (21c)$$

$$\partial_t\phi_{2\Gamma} = -\Gamma_{12}\left[\mathbf{n}\cdot\kappa_1\nabla\phi_1 - \kappa_{1\Gamma}\Delta_\Gamma\phi_{1\Gamma} + \frac{\partial f_s}{\partial\phi_{1\Gamma}}\right] - \Gamma_2\left[\mathbf{n}\cdot\kappa_2\nabla\phi_2 - \kappa_{2\Gamma}\Delta_\Gamma\phi_{2\Gamma} + \frac{\partial f_s}{\partial\phi_{2\Gamma}}\right], \quad (21d)$$

where Γ_1 , Γ_2 and Γ_{12} are the relaxation parameters of dynamic boundary conditions, $M_i(\phi_1, \phi_2)$ and $M_{12}(\phi_1, \phi_2)$ are defined as

$$M_1(\phi_1, \phi_2) = m_1\phi_1(1 - \phi_1 - \phi_2), \quad (22)$$

$$M_2(\phi_1, \phi_2) = m_2\phi_2(1 - \phi_1 - \phi_2), \quad (23)$$

$$M_{12}(\phi_1, \phi_2) = m_{12}\phi_1\phi_2(1 - \phi_1 - \phi_2). \quad (24)$$

to remove the singularity from Flory-Huggins free energy density functions. $M_i(\phi_1, \phi_2)$ and Γ_i , $i = 1, 2$ are the diagonal elements in the mobility matrix, depicting the direct effects of forces on the corresponding fluxes, while $M_{12}(\phi_1, \phi_2)$ and Γ_{12} are the cross coupling terms denoting the cross interplay of forces and fluxes. The cross coupling relaxation rate refers to the rate at which perturbations in one variable are coupled to changes in another variable in the system. We note that our model is an extension of the binary model developed in [17]. Our work provides a general framework that can extend all existing binary mixture models [22, 33, 36, 46] with dynamic boundary conditions to a ternary model.

Combining the definition of fluxes achieved from the Onsager principle with the conservation laws (14), we obtain the governing equations of the system as follows.

$$\partial_t\phi_1 = \nabla M_1(\phi_1, \phi_2)\cdot\nabla\mu_1 + \nabla M_{12}(\phi_1, \phi_2)\cdot\nabla\mu_2, \quad (25a)$$

$$\partial_t\phi_2 = \nabla M_2(\phi_1, \phi_2)\cdot\nabla\mu_2 + \nabla M_{12}(\phi_1, \phi_2)\cdot\nabla\mu_1, \quad (25b)$$

with boundary conditions:

$$\partial_t\phi_{1\Gamma} = -\Gamma_1\left[\mathbf{n}\cdot\kappa_1\nabla\phi_1 - \kappa_{1\Gamma}\Delta_\Gamma\phi_{1\Gamma} + \frac{\partial f_s}{\partial\phi_{1\Gamma}}\right] - \Gamma_{12}\left[\mathbf{n}\cdot\kappa_2\nabla\phi_2 - \kappa_{2\Gamma}\Delta_\Gamma\phi_{2\Gamma} + \frac{\partial f_s}{\partial\phi_{2\Gamma}}\right], \quad (26a)$$

$$\partial_t\phi_{2\Gamma} = -\Gamma_2\left[\mathbf{n}\cdot\kappa_2\nabla\phi_2 - \kappa_{2\Gamma}\Delta_\Gamma\phi_{2\Gamma} + \frac{\partial f_s}{\partial\phi_{2\Gamma}}\right] - \Gamma_{12}\left[\mathbf{n}\cdot\kappa_1\nabla\phi_1 - \kappa_{1\Gamma}\Delta_\Gamma\phi_{1\Gamma} + \frac{\partial f_s}{\partial\phi_{1\Gamma}}\right], \quad (26b)$$

$$\partial_{\mathbf{n}}\mu_1|_\Gamma = 0, \quad (26c)$$

$$\partial_{\mathbf{n}}\mu_2|_\Gamma = 0. \quad (26d)$$

We denote the diffusion coefficients as $D_i = m_i k_B T$, $i = 1, 2$, and $D_{12} = m_{12} k_B T$. In this work, we use the dynamic boundary condition (26) in x -direction and the periodic boundary condition for all variables in y -direction.

Our model has the following properties:

Theorem 2.1 *The total mass of each component in the domain Ω is conserved, i.e.*

$$\int_{\Omega} \phi_i(x, y, t) d\mathbf{x} = \int_{\Omega} \phi_i(x, y, 0) d\mathbf{x}, \quad i = 1, 2. \quad (27)$$

proof: For $i = 1$,

$$\begin{aligned} \frac{d}{dt} \int_{\Omega} \phi_1 d\mathbf{x} &= \int_{\Omega} \partial_t \phi_1 d\mathbf{x} = - \int_{\Omega} \nabla \cdot \mathbf{J}_1 d\mathbf{x} = \int_{\Gamma} \mathbf{J}_1 \cdot \mathbf{n} dS \\ &= \int_{\Gamma} \left[-M_1(\phi_1, \phi_2) \nabla \mu_1 - M_{12}(\phi_1, \phi_2) \nabla \mu_2 \right] \cdot \mathbf{n} dS = 0, \end{aligned} \quad (28)$$

as boundary condition $\partial_{\mathbf{n}} \mu_1|_{\Gamma} = 0$ and $\partial_{\mathbf{n}} \mu_2|_{\Gamma} = 0$. Similar for $i = 2$. Thus Eq. (27) is obtained.

Theorem 2.2 *The total free energy is dissipative, i.e.*

$$\partial_t E = \partial_t (E_{\text{surf}} + E_{\text{bulk}}) \leq 0. \quad (29)$$

proof: For simplicity, we assume $\nu_1 = \nu_2 = \nu$, and we define

$$\mu_{1\Gamma} = \mathbf{n} \cdot \kappa_1 \nabla \phi_1 - \kappa_{1\Gamma} \Delta_{\Gamma} \phi_{1\Gamma} + \frac{\partial f_s}{\partial \phi_{1\Gamma}}, \quad (30)$$

$$\mu_{2\Gamma} = \mathbf{n} \cdot \kappa_2 \nabla \phi_2 - \kappa_{2\Gamma} \Delta_{\Gamma} \phi_{2\Gamma} + \frac{\partial f_s}{\partial \phi_{2\Gamma}}. \quad (31)$$

The total energy dissipation rate reads

$$\begin{aligned} \partial_t E &= \int_{\Omega} dx \left[\left(\frac{\partial f_b}{\partial \phi_1} - \kappa_1 \Delta \phi_1 \right) \partial_t \phi_1 + \left(\frac{\partial f_b}{\partial \phi_2} - \kappa_2 \Delta \phi_2 \right) \partial_t \phi_2 \right] \\ &\quad + \int_{\Gamma} dS \left[\mathbf{n} \cdot \kappa_1 \nabla \phi_1 + \left(\frac{\partial f_s}{\partial \phi_{1\Gamma}} - \kappa_{1\Gamma} \Delta_{\Gamma} \phi_{1\Gamma} \right) \right] \frac{\partial \phi_{1\Gamma}}{\partial t} + \int_{\Gamma} dS \left[\mathbf{n} \cdot \kappa_2 \nabla \phi_2 + \left(\frac{\partial f_s}{\partial \phi_{2\Gamma}} - \kappa_{2\Gamma} \Delta_{\Gamma} \phi_{2\Gamma} \right) \right] \frac{\partial \phi_{2\Gamma}}{\partial t} \\ &= - \int_{\Omega} dx \frac{1}{\nu} \left[M_1(\phi_1, \phi_2) |\nabla \mu_1|^2 + 2M_{12}(\phi_1, \phi_2) \nabla \mu_1 \cdot \nabla \mu_2 + M_2(\phi_1, \phi_2) |\nabla \mu_2|^2 \right] \\ &\quad - \int_{\Gamma} dS \left[\Gamma_1 \mu_{1\Gamma}^2 + 2\Gamma_{12} \mu_{1\Gamma} \mu_{2\Gamma} + \Gamma_2 \mu_{2\Gamma}^2 \right]. \end{aligned} \quad (32)$$

Since mobility matrices $\begin{bmatrix} M_1 & M_{12} \\ M_{12} & M_2 \end{bmatrix}$, $\begin{bmatrix} \Gamma_1 & \Gamma_{12} \\ \Gamma_{12} & \Gamma_2 \end{bmatrix}$ are positive definite, $\partial_t E \leq 0$ holds.

2.2. Non-dimensionalization

We set the characteristic length scale as the molecule length $l_0 = \nu^{1/3}$, characteristic time scale $t_0 = \nu^{2/3}/D_1$ such that $\tilde{D}_1 = D_1 t_0 / l_0^2 = 1$. Rescaling: $\tilde{\mathbf{x}} = \mathbf{x}/l_0$ and $\tilde{t} = t/t_0$, our model has the following nondimensional parameters:

$$\tilde{D}_2 = \frac{D_2}{D_1}, \quad \tilde{D}_{12} = \frac{D_{12}}{D_1}, \quad \tilde{\Gamma}_i = \Gamma_i \frac{k_B T}{\nu_s} t_0, \quad \bar{\kappa}_i = \kappa_i \frac{\nu_s}{k_B T} \frac{1}{l_0} = \frac{\nu^{1/3}}{l_0}, \quad (33)$$

$$\tilde{f}_s = f_s \frac{\nu_s}{k_B T}, \quad \tilde{\kappa}_{i\Gamma} = \frac{1}{l_0^{2/3}} \kappa_{i\Gamma} \frac{\nu_s}{k_B T}, \quad \tilde{\kappa}_i = \frac{1}{l_0^{2/3}} \kappa_i \frac{\nu}{k_B T}, \quad i = 1, 2. \quad (34)$$

For brevity, we skip the tildes in the following. The dimensionless equations governing the kinetics of the system are given as:

$$\partial_t \phi_1 = \nabla \phi_1 (1 - \phi_1 - \phi_2) \cdot \nabla \mu_1 + \nabla D_{12} \phi_1 \phi_2 (1 - \phi_1 - \phi_2) \cdot \nabla \mu_2, \quad (35a)$$

$$\partial_t \phi_2 = \nabla D_{12} \phi_1 \phi_2 (1 - \phi_1 - \phi_2) \cdot \nabla \mu_1 + \nabla D_2 \phi_2 (1 - \phi_1 - \phi_2) \cdot \nabla \mu_2, \quad (35b)$$

with dimensionless boundary conditions are written as:

$$\partial_t \phi_{1\Gamma} = -\Gamma_1 \left[\mathbf{n} \cdot \bar{\kappa}_1 \nabla \phi_1 - \kappa_{1\Gamma} \Delta_\Gamma \phi_{1\Gamma} + \frac{\partial f_s}{\partial \phi_{1\Gamma}} \right] - \Gamma_{12} \left[\mathbf{n} \cdot \bar{\kappa}_2 \nabla \phi_2 - \kappa_{2\Gamma} \Delta_\Gamma \phi_{2\Gamma} + \frac{\partial f_s}{\partial \phi_{2\Gamma}} \right], \quad (36a)$$

$$\partial_t \phi_{2\Gamma} = -\Gamma_2 \left[\mathbf{n} \cdot \bar{\kappa}_2 \nabla \phi_2 - \kappa_{2\Gamma} \Delta_\Gamma \phi_{2\Gamma} + \frac{\partial f_s}{\partial \phi_{2\Gamma}} \right] - \Gamma_{12} \left[\mathbf{n} \cdot \bar{\kappa}_1 \nabla \phi_1 - \kappa_{1\Gamma} \Delta_\Gamma \phi_{1\Gamma} + \frac{\partial f_s}{\partial \phi_{1\Gamma}} \right], \quad (36b)$$

$$\partial_{\mathbf{n}} \mu_1|_\Gamma = 0, \quad (36c)$$

$$\partial_{\mathbf{n}} \mu_2|_\Gamma = 0. \quad (36d)$$

In the next section, we will develop the numerical scheme based on the Invariant Energy Quadratization method[12, 51, 54, 55].

3. NUMERICAL SCHEME

We first reformulate the mathematical model into an equivalent formation. Then we discretize the reformulated system in time and space, respectively. In this work, we consider the 2D domain for simplicity.

3.1. Mathematical reformulation

We reformulate the total free energy in a quadratic form

$$q_1 = \sqrt{\frac{\phi_1}{n_1} \ln \phi_1 + \frac{\phi_2}{n_2} \ln \phi_2 + (1 - \phi_1 - \phi_2) \ln(1 - \phi_1 - \phi_2) + \chi_{12} \phi_1 \phi_2 + \chi_{13} \phi_1 \phi_3 + \chi_{23} \phi_2 \phi_3 + C}, \quad (37)$$

where C is a constant such that the value under the square root is positive, $\phi_3 = 1 - \phi_1 - \phi_2$. Then, the total energy becomes

$$E = E_{\text{surf}} + E_{\text{bulk}} = E_{\text{surf}} + \int_{\Omega} \left[q_1^2 + \omega_1 \phi_1 + \omega_2 \phi_2 + \frac{\kappa_1}{2} |\nabla \phi_1|^2 + \frac{\kappa_2}{2} |\nabla \phi_2|^2 \right] d\mathbf{x}. \quad (38)$$

the chemical potentials become

$$\mu_1 = 2q_1 \frac{\partial q_1}{\partial \phi_1} + \omega_1 - \kappa_1 \Delta \phi_1, \quad (39a)$$

$$\mu_2 = 2q_1 \frac{\partial q_1}{\partial \phi_2} + \omega_2 - \kappa_2 \Delta \phi_2. \quad (39b)$$

The reformulated governing equations of the system are as follows.

$$\partial_t \phi_1 = \nabla M_1(\phi_1, \phi_2) \cdot \nabla \mu_1 + \nabla M_{12}(\phi_1, \phi_2) \cdot \nabla \mu_2, \quad (40a)$$

$$\partial_t \phi_2 = \nabla M_2(\phi_1, \phi_2) \cdot \nabla \mu_2 + \nabla M_{12}(\phi_1, \phi_2) \cdot \nabla \mu_1, \quad (40b)$$

$$\partial_t q_1 = \frac{\partial q_1}{\partial \phi_1} \partial_t \phi_1 + \frac{\partial q_1}{\partial \phi_2} \partial_t \phi_2. \quad (40c)$$

with boundary conditions:

$$\partial_t \phi_{1\Gamma} = -\Gamma_1 \left[\mathbf{n} \cdot \kappa_1 \nabla \phi_1 - \kappa_{1\Gamma} \Delta_{\Gamma} \phi_{1\Gamma} + \frac{\partial f_s}{\partial \phi_{1\Gamma}} \right] - \Gamma_{12} \left[\mathbf{n} \cdot \kappa_2 \nabla \phi_2 - \kappa_{1\Gamma} \Delta_{\Gamma} \phi_{2\Gamma} + \frac{\partial f_s}{\partial \phi_{2\Gamma}} \right], \quad (41a)$$

$$\partial_t \phi_{2\Gamma} = -\Gamma_2 \left[\mathbf{n} \cdot \kappa_2 \nabla \phi_2 - \kappa_{1\Gamma} \Delta_{\Gamma} \phi_{2\Gamma} + \frac{\partial f_s}{\partial \phi_{2\Gamma}} \right] - \Gamma_{12} \left[\mathbf{n} \cdot \kappa_1 \nabla \phi_1 - \kappa_{1\Gamma} \Delta_{\Gamma} \phi_{1\Gamma} + \frac{\partial f_s}{\partial \phi_{1\Gamma}} \right], \quad (41b)$$

$$\partial_n \mu_1|_{\Gamma} = 0, \quad (41c)$$

$$\partial_n \mu_2|_{\Gamma} = 0. \quad (41d)$$

The reformulated system has the following properties.

Theorem 3.1 *The total mass of each component in the domain Ω is conserved, i.e.*

$$\int_{\Omega} \phi_i(x, y, t) d\mathbf{x} = \int_{\Omega} \phi_i(x, y, 0) d\mathbf{x}, \quad i = 1, 2. \quad (42)$$

Theorem 3.2 *The total free energy is dissipative, i.e.*

$$\partial_t E = \partial_t (E_{\text{surf}} + E_{\text{bulk}}) \leq 0. \quad (43)$$

We skip the proof here. Next, we will discretize the reformulated governing equation in both the time and space directions.

3.2. Semi-discrete scheme in time

We use the Crank-Nicolson method in the time direction. Δt is the time step. $(\cdot)^n$ represents the solution at n^{th} time step, i.e. $t_n = n\Delta t$. We denote

$$\partial_t^{n+1}(\cdot) = \frac{(\cdot)^{n+1} - (\cdot)^n}{\Delta t}, \quad (\cdot)^{n+1/2} = \frac{(\cdot)^n + (\cdot)^{n+1}}{2}, \quad (\bar{\cdot})^{n+1/2} = \frac{3(\cdot)^n - (\cdot)^{n-1}}{2}. \quad (44)$$

The governing equations of the system are as follows:

$$\partial_t^{n+1}\phi_1 = \nabla M_1(\bar{\phi}_1^{n+1/2}, \bar{\phi}_2^{n+1/2}) \cdot \nabla \mu_1^{n+1/2} + \nabla M_{12}(\bar{\phi}_1^{n+1/2}, \bar{\phi}_2^{n+1/2}) \cdot \nabla \mu_2^{n+1/2}, \quad (45a)$$

$$\partial_t^{n+1}\phi_2 = \nabla M_2(\bar{\phi}_1^{n+1/2}, \bar{\phi}_2^{n+1/2}) \cdot \nabla \mu_2^{n+1/2} + \nabla M_{12}(\bar{\phi}_1^{n+1/2}, \bar{\phi}_2^{n+1/2}) \cdot \nabla \mu_1^{n+1/2}, \quad (45b)$$

$$\partial_t^{n+1}q_1 = \frac{\partial \bar{q}_1}{\partial \phi_1} \partial_t^{n+1}\phi_1 + \frac{\partial \bar{q}_1}{\partial \phi_2} \partial_t^{n+1}\phi_2. \quad (45c)$$

with boundary conditions:

$$\partial_t^{n+1}\phi_{1\Gamma} = -\Gamma_1 \left[\mathbf{n} \cdot \bar{\kappa}_1 \nabla \phi_1^{n+1/2} - \kappa_{1\Gamma} \Delta_\Gamma \phi_{1\Gamma}^{n+1/2} + \frac{\partial f_s}{\partial \phi_{1\Gamma}} \right] \quad (46a)$$

$$- \Gamma_{12} \left[\mathbf{n} \cdot \bar{\kappa}_2 \nabla \phi_2^{n+1/2} - \kappa_{1\Gamma} \Delta_\Gamma \phi_{2\Gamma}^{n+1/2} + \frac{\partial f_s}{\partial \phi_{2\Gamma}} \right],$$

$$\partial_t^{n+1}\phi_{2\Gamma} = -\Gamma_2 \left[\mathbf{n} \cdot \bar{\kappa}_2 \nabla \phi_2^{n+1/2} - \kappa_{1\Gamma} \Delta_\Gamma \phi_{2\Gamma}^{n+1/2} + \frac{\partial f_s}{\partial \phi_{2\Gamma}} \right] \quad (46b)$$

$$- \Gamma_{12} \left[\mathbf{n} \cdot \bar{\kappa}_1 \nabla \phi_1^{n+1/2} - \kappa_{1\Gamma} \Delta_\Gamma \phi_{1\Gamma}^{n+1/2} + \frac{\partial f_s}{\partial \phi_{1\Gamma}} \right],$$

$$\partial_{\mathbf{n}} \mu_1^{n+1} |_\Gamma = 0, \quad (46c)$$

$$\partial_{\mathbf{n}} \mu_2^{n+1} |_\Gamma = 0. \quad (46d)$$

where

$$\mu_1^{n+1/2} = 2q_1^{n+1/2} \frac{\partial \bar{q}_1}{\partial \phi_1} \quad + \omega_1 - \kappa_1 \Delta \phi_1^{n+1/2}, \quad (47a)$$

$$\mu_2^{n+1/2} = 2q_1^{n+1/2} \frac{\partial \bar{q}_1}{\partial \phi_2} \quad + \omega_2 - \kappa_2 \Delta \phi_2^{n+1/2}. \quad (47b)$$

3.3. Fully discrete scheme

We use central finite difference method such that there is second order accuracy in the space. In specific, We use uniform mesh in two-dimensional space $[0, L] \times [0, L]$ (see Fig. 1). In the x -direction, the domain is divided into N_x equal-sized subintervals. Similarly, in the y -direction, the domain is divided into N_y subintervals, each of equal size. We discretize the scalar functions such

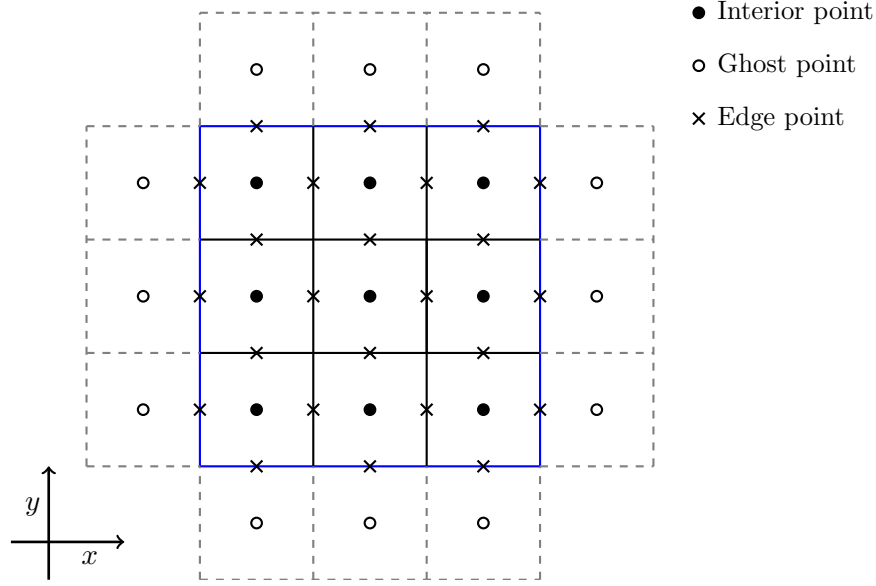


FIG. 1: Sketch of the staggered mesh in two dimensional space. The blue line is the boundary Γ of the 2D domain $\Omega = [0, L] \times [0, L]$ in $x - y$ plane. The black solid points are the center points inside the bulk, the black empty points are the ghost points adjacent to the boundary Γ , and the crosses denote the edge points.

as ϕ_i and $\Delta\phi_i$ values at the center point (x_i, y_j) , where

$$\begin{aligned}
 x_i &= \left(i - \frac{1}{2}\right) \frac{L}{N_x}, & i &= 0, 1, \dots, N_x + 1, \\
 y_j &= \left(j - \frac{1}{2}\right) \frac{L}{N_y}, & j &= 0, 1, \dots, N_y + 1,
 \end{aligned} \tag{48}$$

while discretize the vector functions, e.g. $\nabla\phi_i$ at the edge points $(x_{i+\frac{1}{2}}, y_j)$ or $(x_i, y_{j+\frac{1}{2}})$ [56], where

$$\begin{aligned}
 x_{i+\frac{1}{2}} &= i \frac{L}{N_x}, & i &= 0, 1, \dots, N_x, \\
 y_{j+\frac{1}{2}} &= j \frac{L}{N_y}, & j &= 0, 1, \dots, N_y,
 \end{aligned} \tag{49}$$

At the boundary Γ , we use the average value at adjacent discrete center points. e.g.

$$\phi_{1\Gamma}^n|_{\frac{1}{2},j} = \frac{\phi_1^n|_{0,j} + \phi_1^n|_{1,j}}{2}, \quad \phi_{1\Gamma}^n|_{N_x+\frac{1}{2},j} = \frac{\phi_1^n|_{N_x,j} + \phi_1^n|_{N_x+1,j}}{2}. \tag{50}$$

$j = 1, \dots, N_y$, is the index in y -direction.

We denote the edge-to-center average and difference operator as a_x, d_x in x -direction, a_y, d_y in

y -direction, which are defined as follows

$$a_x u_{i,j} := \frac{1}{2}(u_{i+\frac{1}{2},j} + u_{i-\frac{1}{2},j}), \quad d_x u_{i,j} := \frac{1}{h_x}(u_{i+\frac{1}{2},j} - u_{i-\frac{1}{2},j}), \quad (51)$$

$$a_y v_{i,j} := \frac{1}{2}(v_{i,j+\frac{1}{2}} + v_{i,j-\frac{1}{2}}), \quad d_y v_{i,j} := \frac{1}{h_y}(v_{i,j+\frac{1}{2}} - v_{i,j-\frac{1}{2}}). \quad (52)$$

We denote the center-to-edge average and difference operators by A_x, D_x in x -direction. Analogously, the center-to-edge in y -direction average and difference operators are denoted as A_y, D_y . Their definitions are as follows.

$$A_x \phi_{i+\frac{1}{2},j} := \frac{1}{2}(\phi_{i+1,j} + \phi_{i,j}), \quad D_x \phi_{i+\frac{1}{2},j} := \frac{1}{h_x}(\phi_{i+1,j} - \phi_{i,j}), \quad (53)$$

$$A_y \phi_{i,j+\frac{1}{2}} := \frac{1}{2}(\phi_{i,j+1} + \phi_{i,j}), \quad D_y \phi_{i,j+\frac{1}{2}} := \frac{1}{h_y}(\phi_{i,j+1} - \phi_{i,j}). \quad (54)$$

The standard 2D discrete Laplace operator is defined as Δ_h in the bulk and $\Delta_{\Gamma h}$ on the surface.

$$\Delta_h \phi := d_x(D_x \phi) + d_y(D_y \phi), \quad \Delta_{\Gamma h} \phi_\Gamma := d_y(D_y \phi_\Gamma), \quad \text{or} \quad \Delta_{\Gamma h} \phi_\Gamma := d_x(D_x \phi_\Gamma). \quad (55)$$

The discrete norm in bulk and surface are defined as follows:

$$\|\phi\|_c = h_x h_y \sum_{i=1}^{N_x} \sum_{j=1}^{N_y} \phi_{i,j}, \quad \|\nabla \phi\|_v = h_x h_y \sum_{i=1}^{N_x} \sum_{j=1}^{N_y} \left[a_x D_x \phi_{i+\frac{1}{2},j} + a_y D_y \phi_{i,j+\frac{1}{2}} \right], \quad (56)$$

$$\|\phi\|_{c,\Gamma} = h_y \sum_{j=1}^{N_y} \phi_{j,\Gamma}, \quad \|\nabla \phi\|_{v,\Gamma} = h_y \sum_{j=1}^{N_y} \left[a_y D_y \phi_{i,j+\frac{1}{2}} \right]. \quad (57)$$

The fully discrete numerical scheme:

$$\left\{ \begin{aligned} \partial_t^{n+1} \phi_1 &= d_x A_x (M_1(\bar{\phi}_1^{n+1/2}, \bar{\phi}_2^{n+1/2})) D_x \mu_1^{n+1/2} + d_y A_y (M_1(\bar{\phi}_1^{n+1/2}, \bar{\phi}_2^{n+1/2})) D_y \mu_1^{n+1/2} \\ &+ d_x A_x (M_{12}(\bar{\phi}_1^{n+1/2}, \bar{\phi}_2^{n+1/2})) D_x \mu_2^{n+1/2} + d_y A_y (M_{12}(\bar{\phi}_1^{n+1/2}, \bar{\phi}_2^{n+1/2})) D_y \mu_2^{n+1/2} \end{aligned} \right\} \Big|_{i,j}, \quad (58)$$

$$\left\{ \begin{aligned} \partial_t^{n+1} \phi_2 &= d_x A_x (M_2(\bar{\phi}_1^{n+1/2}, \bar{\phi}_2^{n+1/2})) D_x \mu_2^{n+1/2} + d_y A_y (M_2(\bar{\phi}_1^{n+1/2}, \bar{\phi}_2^{n+1/2})) D_y \mu_2^{n+1/2} \\ &+ d_x A_x (M_{12}(\bar{\phi}_1^{n+1/2}, \bar{\phi}_2^{n+1/2})) D_x \mu_1^{n+1/2} + d_y A_y (M_{12}(\bar{\phi}_1^{n+1/2}, \bar{\phi}_2^{n+1/2})) D_y \mu_1^{n+1/2} \end{aligned} \right\} \Big|_{i,j}, \quad (59)$$

$$\left\{ \partial_t^{n+1} q_1 = \frac{\partial \bar{q}_1}{\partial \phi_1} \partial_t^{n+1} \phi_1 + \frac{\partial \bar{q}_1}{\partial \phi_2} \partial_t^{n+1} \phi_2 \right\} \Big|_{i,j}. \quad (60)$$

where $i = 1, \dots, N_x$, $j = 1, \dots, N_y$. with boundary conditions:

$$\left\{ \begin{aligned} \partial_t^{n+1} \phi_{1\Gamma} &= -\Gamma_1 \left[\mathbf{n} \cdot \bar{\kappa}_1 d_x \phi_1^{n+1/2} - \kappa_{1\Gamma} \Delta_{\Gamma h} \phi_{1\Gamma}^{n+1/2} + \frac{\partial f_s}{\partial \phi_{1\Gamma}} \right]^{n+1/2} \\ &\quad - \Gamma_{12} \left[\mathbf{n} \cdot \bar{\kappa}_2 d_x \phi_2^{n+1/2} - \kappa_{2\Gamma} \Delta_{\Gamma h} \phi_{2\Gamma}^{n+1/2} + \frac{\partial f_s}{\partial \phi_{2\Gamma}} \right]^{n+1/2} \end{aligned} \right\} \Big|_{\frac{1}{2} \text{ or } (N_x + \frac{1}{2}), j}, \quad (61a)$$

$$\left\{ \begin{aligned} \partial_t^{n+1} \phi_{2\Gamma} &= -\Gamma_2 \left[\mathbf{n} \cdot \bar{\kappa}_2 d_x \phi_2^{n+1/2} - \kappa_{2\Gamma} \Delta_{\Gamma h} \phi_{2\Gamma}^{n+1/2} + \frac{\partial f_s}{\partial \phi_{2\Gamma}} \right]^{n+1/2} \\ &\quad - \Gamma_{12} \left[\mathbf{n} \cdot \bar{\kappa}_1 d_x \phi_1^{n+1/2} - \kappa_{1\Gamma} \Delta_{\Gamma h} \phi_{1\Gamma}^{n+1/2} + \frac{\partial f_s}{\partial \phi_{1\Gamma}} \right]^{n+1/2} \end{aligned} \right\} \Big|_{\frac{1}{2} \text{ or } (N_x + \frac{1}{2}), j}, \quad (61b)$$

$$\mu_k|_{0,j} = \mu_k|_{1,j}, \quad \mu_k|_{N_x,j} = \mu_k|_{N_x+1,j}, \quad k = 1, 2. \quad (61c)$$

$$\mu_k|_{i,0} = \mu_k|_{i,1}, \quad \mu_k|_{i,N_y} = \mu_k|_{i,N_y+1}, \quad k = 1, 2, \quad (61d)$$

where

$$\mu_1^{n+1/2}|_{i,j} = 2q_1|_{i,j}^{n+1/2} \frac{\partial \bar{q}_1}{\partial \phi_1} \Big|_{i,j} + \omega_1 - \kappa_1 \Delta_h \phi_1^{n+1/2}|_{i,j}, \quad (62a)$$

$$\mu_2^{n+1/2}|_{i,j} = 2q_1|_{i,j}^{n+1/2} \frac{\partial \bar{q}_1}{\partial \phi_2} \Big|_{i,j} + \omega_2 - \kappa_2 \Delta_h \phi_2^{n+1/2}|_{i,j}. \quad (62b)$$

The fully discrete numerical scheme fulfills the total mass conservation law and the total energy dissipation rate at the discrete level.

Theorem 3.3 *Mass conservation law at discrete level: Based on the discrete boundary conditions (61)*

$$\sum_{i=1}^{N_x} \sum_{j=1}^{N_y} \frac{\phi_1^{n+1}|_{i,j} - \phi_1^n|_{i,j}}{\Delta t} = \sum_{i=1}^{N_x} \sum_{j=1}^{N_y} \left[\nabla \cdot M_1 \nabla \mu_1^{n+1/2}|_{i,j} + \nabla \cdot M_{12} \nabla \mu_2^{n+1/2}|_{i,j} \right] = 0. \quad (63)$$

same as for the total mass of ϕ_2 .

Theorem 3.4 *Unconditionally energy stability at discrete level: The discrete energy of the system is defined as:*

$$E^{n+1} = E_{\text{bulk}}^{n+1} + E_{\text{surf}}^{n+1}, \quad (64)$$

where

$$E_{\text{bulk}}^{n+1} = \|f_b(\phi_1, \phi_2)^{n+1}\|_c + \frac{\kappa_1}{2} \|\nabla \phi_1^{n+1}\|_v^2 + \frac{\kappa_2}{2} \|\nabla \phi_2^{n+1}\|_v^2, \quad (65)$$

$$E_{\text{surf}}^{n+1} = \|f_s(\phi_{1\Gamma}, \phi_{2\Gamma})^{n+1}\|_{c,\Gamma} + \frac{\kappa_{1\Gamma}}{2} \|\nabla \phi_{1\Gamma}^{n+1}\|_{v,\Gamma}^2 + \frac{\kappa_{2\Gamma}}{2} \|\nabla \phi_{2\Gamma}^{n+1}\|_{v,\Gamma}^2. \quad (66)$$

The total energy at discrete level decreases with respect to time, i.e.

$$E^{n+1} \leq E^n. \quad (67)$$

proof: Using the definition of reformulated total energy at discrete level (64) and the formula $(a^2 - b^2) = (a + b)(a - b)$ we obtain,

$$\begin{aligned}
\frac{E^{n+1} - E^n}{\Delta t} = & \|2 \cdot \frac{q_1^{n+1} - q_1^n}{\Delta t} \frac{q_1^{n+1} + q_1^n}{2} + \omega_1 \frac{\phi_1^{n+1} - \phi_1^n}{\Delta t} + \omega_2 \frac{\phi_2^{n+1} - \phi_2^n}{\Delta t}\|_c \\
& + \frac{\kappa_1}{2} \|2 \cdot \frac{\nabla \phi_1^{n+1} - \nabla \phi_1^n}{\Delta t} \frac{\nabla \phi_1^{n+1} + \nabla \phi_1^n}{2}\|_v + \frac{\kappa_2}{2} \|2 \cdot \frac{\nabla \phi_2^{n+1} - \nabla \phi_2^n}{\Delta t} \frac{\nabla \phi_2^{n+1} + \nabla \phi_2^n}{2}\|_v \\
& + \frac{\kappa_{1\Gamma}}{2} \|2 \cdot \frac{\nabla_{\parallel} \phi_{1\Gamma}^{n+1} - \nabla_{\parallel} \phi_{1\Gamma}^n}{\Delta t} \frac{\nabla_{\parallel} \phi_{1\Gamma}^{n+1} + \nabla_{\parallel} \phi_{1\Gamma}^n}{2}\|_{v,\Gamma} \\
& + \frac{\kappa_{2\Gamma}}{2} \|2 \cdot \frac{\nabla_{\parallel} \phi_{2\Gamma}^{n+1} - \nabla_{\parallel} \phi_{2\Gamma}^n}{\Delta t} \frac{\nabla_{\parallel} \phi_{2\Gamma}^{n+1} + \nabla_{\parallel} \phi_{2\Gamma}^n}{2}\|_{v,\Gamma} \\
& + h_1 \|\frac{\phi_1^{n+1} - \phi_1^n}{\Delta t}\|_c + g_1 \|2 \cdot \frac{\phi_1^{n+1} - \phi_1^n}{\Delta t} \frac{\phi_1^{n+1} + \phi_1^n}{2}\|_c \\
& + h_2 \|\frac{\phi_2^{n+1} - \phi_2^n}{\Delta t}\|_c + g_2 \|\frac{\phi_2^{n+1} - \phi_2^n}{\Delta t} \frac{\phi_2^{n+1} + \phi_2^n}{2}\|_c \\
& + \gamma \|\frac{\phi_1^{n+1} + \phi_1^n}{2} \frac{\phi_2^{n+1} - \phi_2^n}{\Delta t}\|_c + \gamma \|\frac{\phi_2^{n+1} + \phi_2^n}{2} \frac{\phi_1^{n+1} - \phi_1^n}{\Delta t}\|_c. \tag{68}
\end{aligned}$$

According to the discrete chemical potentials (62) and discrete boundary conditions (61) we have

$$\begin{aligned}
\frac{E^{n+1} - E^n}{\Delta t} = & \|\mu_1^{n+1/2} \cdot (\nabla M_1 \cdot \nabla \mu_1^{n+1/2} + \nabla M_{12} \cdot \nabla \mu_2^{n+1/2})\|_v \\
& + \|\mu_2^{n+1/2} \cdot (\nabla M_2 \cdot \nabla \mu_2^{n+1/2} + \nabla M_{12} \cdot \nabla \mu_1^{n+1/2})\|_v \\
& + \|\mu_{1\Gamma}^{n+1/2} \cdot (-\Gamma_1 \mu_{1\Gamma}^{n+1/2} - \Gamma_{12} \mu_{2\Gamma}^{n+1/2})\|_{v,\Gamma} \\
& + \|\mu_{2\Gamma}^{n+1/2} \cdot (-\Gamma_2 \mu_{2\Gamma}^{n+1/2} - \Gamma_{12} \mu_{1\Gamma}^{n+1/2})\|_{v,\Gamma} \\
= & -\|M_1 |\nabla \mu_1^{n+1/2}|^2 + 2M_{12} \nabla \mu_1^{n+1/2} \cdot \nabla \mu_2^{n+1/2} + M_2 |\nabla \mu_2^{n+1/2}|^2\|_v \\
& - \|\Gamma_1 |\mu_{1\Gamma}^{n+1/2}|^2 + 2\Gamma_{12} \mu_{1\Gamma}^{n+1/2} \mu_{2\Gamma}^{n+1/2} + \Gamma_2 |\mu_{2\Gamma}^{n+1/2}|^2\|_{v,\Gamma} \leq 0. \tag{69}
\end{aligned}$$

i.e. Eq. (67) is obtained.

4. PHYSICAL PHENOMENA INVESTIGATION BY NUMERICAL SIMULATIONS

Taking advantages of numerical simulations on its ability to vary parameter in a controlled manner and over a wide range of scales, we investigate several physical phenomena in this section, including the wettability of multi-component droplets on solid surfaces, the effects of wall-mixture interactions on patterns in the bulk, and the role of cross-coupling relaxation rates in controlling kinetic processes in both the bulk and surface.

According to the Gibbs's rule, a ternary mixture system can have at most three coexisting phases in a system (see Appendix 6.6.1 for details). In this section, we will evidence our points in both two-phase and three-phase coexisting scenarios.

4.1. Wettability, i.e. the contact angle is determined by the additive effects of wall-mixture interaction

The contact angle is a measure of the wetting behavior of a liquid on a solid surface. It is determined by the balance of forces between the solid phase, and other two liquid phases on the top of the solid surface. The wall-mixture interaction plays a significant role in determining the contact angle. In the case of a multi-component liquid mixture, the contact angle is determined by the combined effects of the interactions between the individual component of the mixture and the solid surface. To grasp these additive effects, we define the surface free energy as the summation of interactions between individual component and the solid wall.

Specifically, the surface free energy reads

$$f_s(\phi_{1\Gamma}, \phi_{2\Gamma}) = \frac{k_B T}{\nu_s} \left[h_1 \phi_{1\Gamma} + g_1 \phi_{1\Gamma}^2 + h_2 \phi_{2\Gamma} + g_2 \phi_{2\Gamma}^2 + \gamma \phi_{1\Gamma} \phi_{2\Gamma} \right], \quad (70)$$

Here, $h_i \phi_i$ depicts the interaction between solid wall and i -th component, $g_i \phi_i^2$ represents the interaction among i -th component molecules near by the solid surface. $\gamma \phi_1 \phi_2$ denotes the interaction between different kinds of molecules.

If all the interactions mentioned above are mutual, i.e. $h_i = g_i = \gamma = 0$, the contact angle of droplets on the surface is 90° (see Fig. 2-e). If the interactions between each component and solid wall are all attractive, i.e. $h_i < 0$, $g_i < 0$ or $\gamma < 0$, the contact angle will decrease until complete wetting (see Fig 2, 3, 4, 5-g, and Fig. 6-(a,b)), while repulsive interactions will lead to larger contact angle, i.e. $\theta > 90^\circ$ (see Fig 2, 3, 4, 5-c). If interactions between individual component and solid wall are different, e.g. the interaction between ϕ_1 and solid wall is attractive, while the interaction between ϕ_2 and the solid wall is repulsive, the effective interaction between droplet and solid wall is determined by the dominant component which has high a higher concentration in the droplet (see Fig 2, 3, 4, 5-(a,i)). These observations can be verified in the three phases coexisting (see Appendix) wetting phenomena (see Fig. 7, 8).

4.2. Wall-mixture interaction changes the condensates patterns far away from the surface

The influence of wall-mixture interactions in the formation of condensate patterns in systems exhibiting three-phase coexistence has yet to be extensively investigated. This study aims to bridge this gap by delving into the phase separation and condensates coarsening processes within such systems, paying a special attention to the varying types of wall-mixture interactions.

Our numerical studies revealed that interactions between the wall and the mixture exert a profound effect on the condensate patterns in the bulk, even in regions distant from the surface. We observed distinct variations in the condensate configurations contingent on the nature of the wall-mixture interactions. For instance, in cases where strong attractive or repulsive forces were at play, the resultant patterns manifested as strips running parallel to the solid wall, as evidenced by Fig.10 and Fig.11-(a, b, c, d). Conversely, when the interactions were weak, the patterns that emerged were less structured and more sporadic, as can be seen in Fig.10 and Fig.11-e. These findings underscore the significance of wall-mixture interactions in determining the arrangement of condensates within the bulk.

4.3. Relaxation rate controls the kinetic process in the bulk and surface

The relaxation rate serves as a pivotal factor influencing the kinetic processes occurring within the bulk and on the surface of a system. To elucidate the impact of kinetic rates in the spreading of droplets on a solid surface, we placed a droplet atop the surface and varied the kinetic rates, denoted as Γ_i , from 10^{-4} to 1. Our observations revealed that the surface relaxation rates play a decisive role in dictating the kinetics of droplet spreading. Specifically, a faster surface relaxation rate accelerates the spreading of the droplet, as depicted in Fig. 9.

The exploration of the effects of cross-coupling coefficients has been limited in previous research. In this study, we altered the cross-coupling coefficient, M_{12} , in the bulk to investigate its impact on the phase separation process therein. Our simulations indicate that changes in cross-coupling can indeed alter the kinetic processes (see Fig.12 and Fig.13 for the snapshots). Total mass of ϕ_1 and ϕ_2 (see Fig. 14) with different cross-coupling coefficient M_{12} values are constants as proved by Theorem 3.3. From the total energy profiles (see Fig. 15), it is evident that variations in M_{12} influence the total energy evolution during the initial stages of spontaneous phase separation. Further, we adjusted the cross-coupling coefficient on the surface, Γ_{12} , to scrutinize its effects on the kinetics of droplet spreading on the solid surface. Our findings suggest that cross-coupling exerts a minimal effect on droplet spreading and coarsening subsequent to the phase separation process.

5. CONCLUSIONS

In this paper, we have presented a systematic derivation of multi-component multi-phase mixtures with dynamic boundary conditions. The governing equations in the models are composed of the mass conservation as well as the constitutive equations, which are derived using the Onsager principle to preserve the energy dissipation rate in time. The gradient flow structure is $H^{-1}(\Omega)$ in the bulk and $L_2(\Gamma)$ on the surface.

Moreover, we have presented a second order, fully-discrete, linear and unconditionally energy stable numerical scheme for the ternary mixture model with dynamic boundary conditions. Firstly, we reformulate the model by introducing an intermediate variables following the Energy Quadratization strategy. Using the reformulated model equations, we develop a second order, energy stable, semi-discrete numerical scheme in time. Then, we obtain a fully-discrete numerical scheme by applying the finite difference method on the staggered grid in space, which preserves a fully discrete energy dissipation rate and total mass conservation laws.

Beyond theoretical advancements, our work has substantial engineering implications. Utilizing our efficient and accurate numerical solver, we investigate the effects of short-ranged interaction between mixture components and solid surface on the wettability of the surface, from the perspectives of both stationary and kinetic solutions. We find that the contact angle of condensates are determined by the additive effects introduced by the interaction between each component and solid wall. The droplet spreading can be affected hugely by the surface relaxation rates, while the cross-coupling relaxation rate in the surface does not influence the droplet spreading a lot. Furthermore, the spontaneous phase separation phenomena of ternary mixture with two phases and three phases, with dynamic boundary conditions are explored. Our results suggest that strong attractive/repulsive coupling between surface and bulk leads to ordered condensates patterns in the bulk. Moreover, the cross-coupling in the bulk changes the phase separation process significantly. This insight is invaluable in fields like semiconductor manufacturing, where surface properties are critical, or in medical device fabrication, where understanding biofluid interactions with surfaces can lead to better product designs.

Furthremore, our model and the scheme can be readily extended to models of N -component mixtures with $N > 3$. Our work provides a general framework for the study of multi-component mixture with dynamic boundary conditions. The multi-component mixture with more complex boundary conditions(DBC), e.g. Goldstein DBC (6), Liu-Wu model DBC (7) and KLLM model DBC (8) can be studied based on this framework. This work not only provides a foundational

framework for future study of multi-component mixtures with dynamic boundary conditions for a wide range of applications but also makes a significant influence in the study of complex fluid dynamics.

ACKNOWLEDGEMENT

We thank C. A. Weber and Z. Zhang for insightful discussions. We also thank the anonymous referees for their critical comments.

6. APPENDIX

6.1. Phase diagram of ternary mixture

We use convex hull algorithm to calculate the phase diagram of the ternary mixture. The interaction parameters values are $\chi_{12} = \chi_{23} = \chi_{13} = 3$, the wall-mixture interaction coefficients: $h_1 = h_2 = g_1 = g_2 = \gamma = 0$.

In the phase diagram Fig 16, the x-axis represents the composition of one of the components ϕ_1 in the mixture, while the y-axis represents the composition of another component ϕ_2 . The concentration of third component equals to $1 - \phi_1 - \phi_2$ based on the incompressibility assumption. This phase diagram depicts the behavior of ternary mixture at equilibrium. The black regions represent the mixture which has no phase separation at equilibrium. The ternary mixture which has the compositions at light green regions will phase separate into two coexisting phases with different composition profiles. In the blue region, there are three coexisting phases. The composition of these three phases are denoted by the yellow stars in the three corners of the region. Here, we give three examples of three phase coexisting ternary mixture which are depicted by three colorful dots (red, magenta, blue). Correspondingly, in the Fig. 16-(b.1-b.2, c.1-c.2, d.1-d.2), we show the three phases coexisting system with phases 1, 2, 3. In specific, the Fig. 16-(b.1, c.1, d.1) denotes the concentration profiles of ϕ_1 in each case, while Fig. 16-(b.2, c.2, d.2) the concentration profiles of ϕ_2 . All the numerical studies of three-phases coexisting phenomena in the main text are based on this phase diagram.

TABLE I: Abbreviations

Abbreviations	Explanations
DBC	Dynamic Boundary Condition
IEQ	Invariant Energy Quadraticization

6.2. Abbreviations and Notations

REFERENCES

- [1] Jaime Agudo-Canalejo, Sebastian W. Schultz, Haruka Chino, Simona M. Migliano, Chieko Saito, Ikuko Koyama-Honda, Harald Stenmark, Andreas Brech, Alexander I. May, Noboru Mizushima, and Roland L. Knorr. Wetting regulates autophagy of phase-separated compartments and the cytosol. *Nature*, 591:142–146, 2021.
- [2] A.Lamorgese and R.Mauri. Diffusion-driven dissolution or growth of a liquid drop embedded in a continuous phase of another liquid via phase-field ternary mixture model. *Langmuir*, 33(45):13125–13132, 2017.
- [3] A.Lamorgese and R.Mauri. Dissolution or growth of a liquid drop via phase-field ternary mixture model based on the non-random, two-liquid equation. *Entropy*, 20:125, 02 2018.
- [4] F. Bai, C.M. Elliott, A. Gardiner, A. Spence, and A.M. Stuart. The viscous cahn–hilliard equation. i. computations. *Nonlinearity*, 8:131–160, 1995.
- [5] K. Binder and H. L. Frisch. Dynamics of surface enrichment: A theory based on the kawasaki spin-exchange model in the presence of a wall. *Zeitschrift für Physik B Condensed Matter*, 84(3):403–418, 1991.
- [6] Clifford P. Brangwynne, Christian R. Eckmann, David S. Courson, Agata Rybarska, Carsten Hoege, Jöbin Gharakhani, Frank Jülicher, and Anthony A. Hyman. Germline p granules are liquid droplets that localize by controlled dissolution/condensation. *Science*, 324(5935):1729–1732, 2009.
- [7] F. Bruder and R. Brenn. Spinodal decomposition in thin films of a polymer blend. *Phys. Rev. Lett.*, 69:624–627, Jul 1992.
- [8] P. Gao C. Zhang, H. Ding and Y. Wu. Diffuse interface simulation of ternary fluids in contact with solid. *Journal of Computational Physics*, 309:37–51, 2016.
- [9] John W Cahn. On spinodal decomposition in cubic crystals. *Acta Metallurgica*, 10(3):179–183, 1962.
- [10] John W. Cahn. Critical point wetting. *The Journal of Chemical Physics*, 66(8):3667–3672, 1977.
- [11] John W. Cahn and John E. Hilliard. Free energy of a nonuniform system. i. interfacial free energy. *The Journal of Chemical Physics*, 28(2):258–267, 1958.
- [12] Nicolas Crouseilles, Shi Jin, and Mohammed Lemou. Nonlinear geometric optics method-based multi-

- scale numerical schemes for a class of highly oscillatory transport equations. *Mathematical Models and Methods in Applied Sciences*, 27(11):2031–2070, 2017.
- [13] Masao Doi. Onsager principle in polymer dynamics. *Progress in Polymer Science*, 112:101339, 2021.
- [14] Andrea Ferrari, Joaquin Jimenez-Martinez, Tanguy Le Borgne, Yves Méheust, and Ivan Lunati. Challenges in modeling unstable two-phase flow experiments in porous micromodels. *Water Resources Research*, 51(3):1381–1400, 2015.
- [15] Andrea Ferrari and Ivan Lunati. Direct numerical simulations of interface dynamics to link capillary pressure and total surface energy. *Advances in Water Resources*, 57:19–31, 2013.
- [16] Andrea Ferrari and Ivan Lunati. Inertial effects during irreversible meniscus reconfiguration in angular pores. *Advances in Water Resources*, 74:1–13, 2014.
- [17] Hans Peter Fischer, Philipp Maass, and Wolfgang Dieterich. Novel surface modes in spinodal decomposition. *Phys. Rev. Lett.*, 79:893–896, Aug 1997.
- [18] Eliot Fried and Morton E. Gurtin. Continuum theory of thermally induced phase transitions based on an order parameter. *Physica D: Nonlinear Phenomena*, 68(3):326–343, 1993.
- [19] Takeshi Fukao, Shuji Yoshikawa, and Saori Wada. Structure-preserving finite difference schemes for the cahn-hilliard equation with dynamic boundary conditions in the one-dimensional case. *Communications on Pure and Applied Analysis*, 16(5):1915–1938, 2017.
- [20] Joseph G. Gall, Michel Bellini, Zheng’an Wu, and Christine Murphy. Assembly of the nuclear transcription and processing machinery: Cajal bodies (coiled bodies) and transcriptosomes. *Molecular Biology of the Cell*, 10(12):4385–4402, 1999.
- [21] Harald Garcke, Patrik Knopf, and Sema Yayla. Long-time dynamics of the cahn–hilliard equation with kinetic rate dependent dynamic boundary conditions. *Nonlinear Analysis*, 215:112619, 2022.
- [22] Gisèle Ruiz Goldstein, Alain Miranville, and Giulio Schimperna. A cahn–hilliard model in a domain with non-permeable walls. *Physica D: Nonlinear Phenomena*, 240(8):754–766, 2011.
- [23] Andrew K. Gunstensen, Daniel H. Rothman, Stéphane Zaleski, and Gianluigi Zanetti. Lattice boltzmann model of immiscible fluids. *Phys. Rev. A*, 43:4320–4327, Apr 1991.
- [24] Morton E. Gurtin. Generalized ginzburg-landau and cahn-hilliard equations based on a microforce balance. *Physica D: Nonlinear Phenomena*, 92(3):178–192, 1996.
- [25] Y. Li J. Yang and J. Kim. Modified multi-phase diffuse-interface model for compound droplets in contact with solid. *Journal of Computational Physics*, 491:112345, 2023.
- [26] R. Mauri J.M. Park and P.D. Anderson. Phase separation of viscous ternary liquid mixtures. *Chemical Engineering Science*, 80:270–278, 2012.
- [27] Frank Jülicher and Jacques Prost. Generic theory of colloidal transport. *The European physical journal. E, Soft matter*, 29:27–36, 05 2009.
- [28] R. Kenzler, F. Eurich, P. Maass, B. Rinn, J. Schropp, E. Bohl, and W. Dieterich. Phase separation in confined geometries: Solving the cahn–hilliard equation with generic boundary conditions. *Computer Physics Communications*, 133(2):139–157, 2001.

- [29] Georg Krausch, Chi-An Dai, Edward J. Kramer, and Frank S. Bates. Real space observation of dynamic scaling in a critical polymer mixture. *Phys. Rev. Lett.*, 71:3669–3672, Nov 1993.
- [30] Zi Li, Sergio Galindo-Torres, Alexander Scheuermann, and Ling Li. Mesoscopic approach to fluid-solid interaction: Apparent liquid slippage and its effect on permeability estimation. *Phys. Rev. E*, 98:052803, Nov 2018.
- [31] Zi Li, Jiawei Li, Guanxi Yan, Sergio Galindo-Torres, Alexander Scheuermann, and Ling Li. Mesoscopic model framework for liquid slip in a confined parallel-plate flow channel. *Phys. Rev. Fluids*, 6:034203, Mar 2021.
- [32] H. Liang, J. Xu, J. Chen, Z. Chai, and B. Shi. Lattice boltzmann modeling of wall-bounded ternary fluid flows. *Applied Mathematical Modelling*, 73:487–513, 2019.
- [33] Chun Liu and Hao Wu. An energetic variational approach for the cahn–hilliard equation with dynamic boundary condition: Model derivation and mathematical analysis. *Archive for Rational Mechanics and Analysis*, 233:167–247, 2019.
- [34] L. Onsager. Reciprocal relations in irreversible processes I. *Physical Review*, 37:405–426, 1931.
- [35] L. Onsager. Reciprocal relations in irreversible processes II. *Physical Review*, 38:2265–2279, 1931.
- [36] Chun Liu Patrik Knopf, Kei Fong Lam and Stefan Metzger. Phase-field dynamics with transfer of materials: The cahn–hilliard equation with reaction rate dependent dynamic boundary conditions. *ESAIM*, 55(1):229 – 282, 2021.
- [37] Sanjay Puri and Kurt Binder. Surface effects on spinodal decomposition in binary mixtures and the interplay with wetting phenomena. *Phys. Rev. E*, 49:5359–5377, Jun 1994.
- [38] Sebastian Schmieschek and Jens Harting. Contact angle determination in multicomponent lattice boltzmann simulations. *Communications in Computational Physics*, 9(5):1165–1178, 2011.
- [39] Xiaowen Shan and Hudong Chen. Lattice boltzmann model for simulating flows with multiple phases and components. *Phys. Rev. E*, 47:1815–1819, Mar 1993.
- [40] Xiaowen Shan and Hudong Chen. Simulation of nonideal gases and liquid-gas phase transitions by the lattice boltzmann equation. *Phys. Rev. E*, 49:2941–2948, Apr 1994.
- [41] Ping Sheng, Jianwei Zhang, and Chun Liu. Onsager Principle and Electrorheological Fluid Dynamics. *Progress of Theoretical Physics Supplement*, 175:131–143, 05 2008.
- [42] L. Sung, A. Karim, J. F. Douglas, and C. C. Han. Dimensional crossover in the phase separation kinetics of thin polymer blend films. *Phys. Rev. Lett.*, 76:4368–4371, Jun 1996.
- [43] Michael R. Swift, E. Orlandini, W. R. Osborn, and J. M. Yeomans. Lattice boltzmann simulations of liquid-gas and binary fluid systems. *Phys. Rev. E*, 54:5041–5052, Nov 1996.
- [44] Michael R. Swift, W. R. Osborn, and J. M. Yeomans. Lattice boltzmann simulation of nonideal fluids. *Phys. Rev. Lett.*, 75:830–833, Jul 1995.
- [45] P. Tabeling. Introduction to microfluidics. *Oxford University Press*, 2005.
- [46] Hao Wu. A review on the cahn–hilliard equation: classical results and recent advances in dynamic boundary conditions. *Electronic Research Archive*, 30(8):2788–2832, 2022.

- [47] Zhengru Zhang Xiangjun Meng, Xuelian Bao. Second order stabilized semi-implicit scheme for the cahn-hilliard model with dynamic boundary conditions. *arXiv:2206.07325*, 2022.
- [48] J. Choi Y. Li and J. Kim. Multi-component cahn–hilliard system with different boundary conditions in complex domains. *Journal of Computational Physics*, 323:1–16, 2016.
- [49] Guanxi Yan, Zi Li, Thierry Bore, Sergio Andres Galindo Torres, Alexander Scheuermann, and Ling Li. A lattice boltzmann exploration of two-phase displacement in 2d porous media under various pressure boundary conditions. *Journal of Rock Mechanics and Geotechnical Engineering*, 14(6):1782–1798, 2022.
- [50] Guanxi Yan, Zi Li, Thierry Bore, Sergio Andres Galindo Torres, Alexander Scheuermann, and Ling Li. Discovery of dynamic two-phase flow in porous media using two-dimensional multiphase lattice boltzmann simulation. *Energies*, 14(13), 2021.
- [51] X. Yang and D. Han. Linearly first- and second-order, unconditionally energy stable schemes for the phase field crystal equation. *Journal of Computational Physics*, 333:1116–1134, 2017.
- [52] X. Yang, J. Li, G. Forest, and Q. Wang. Hydrodynamic theories for flows of active liquid crystals and the generalized onsager principle. *Entropy*, 18(6):202, 2016.
- [53] Xiaofeng Yang, Jia Zhao, Qi Wang, and Jie Shen. Numerical approximations for a three-component cahn–hilliard phase-field model based on the invariant energy quadratization method. *Mathematical Models and Methods in Applied Sciences*, 27(11):1993–2030, 2017.
- [54] Jia Zhao, Xiaofeng Yang, Yuezheng Gong, Xueping Zhao, Xiaogang Yang, Jun Li, and Qi Wang. A general strategy for numerical approximations of non-equilibrium models-part i: Thermodynamical systems. *International Journal of Numerical Analysis & Modeling*, 15(6):884–918, 2018.
- [55] Jia Zhao, Xiaofeng Yang, Jun Li, and Qi Wang. Energy stable numerical schemes for a hydrodynamic model of nematic liquid crystals. *SIAM. J. Sci. Comput.*, 38:A3264–A3290, 2016.
- [56] Xueping Zhao and Qi Wang. A second order fully-discrete linear energy stable scheme for a binary compressible viscous fluid model. *Journal of Computational Physics*, 395:382–409, 2019.

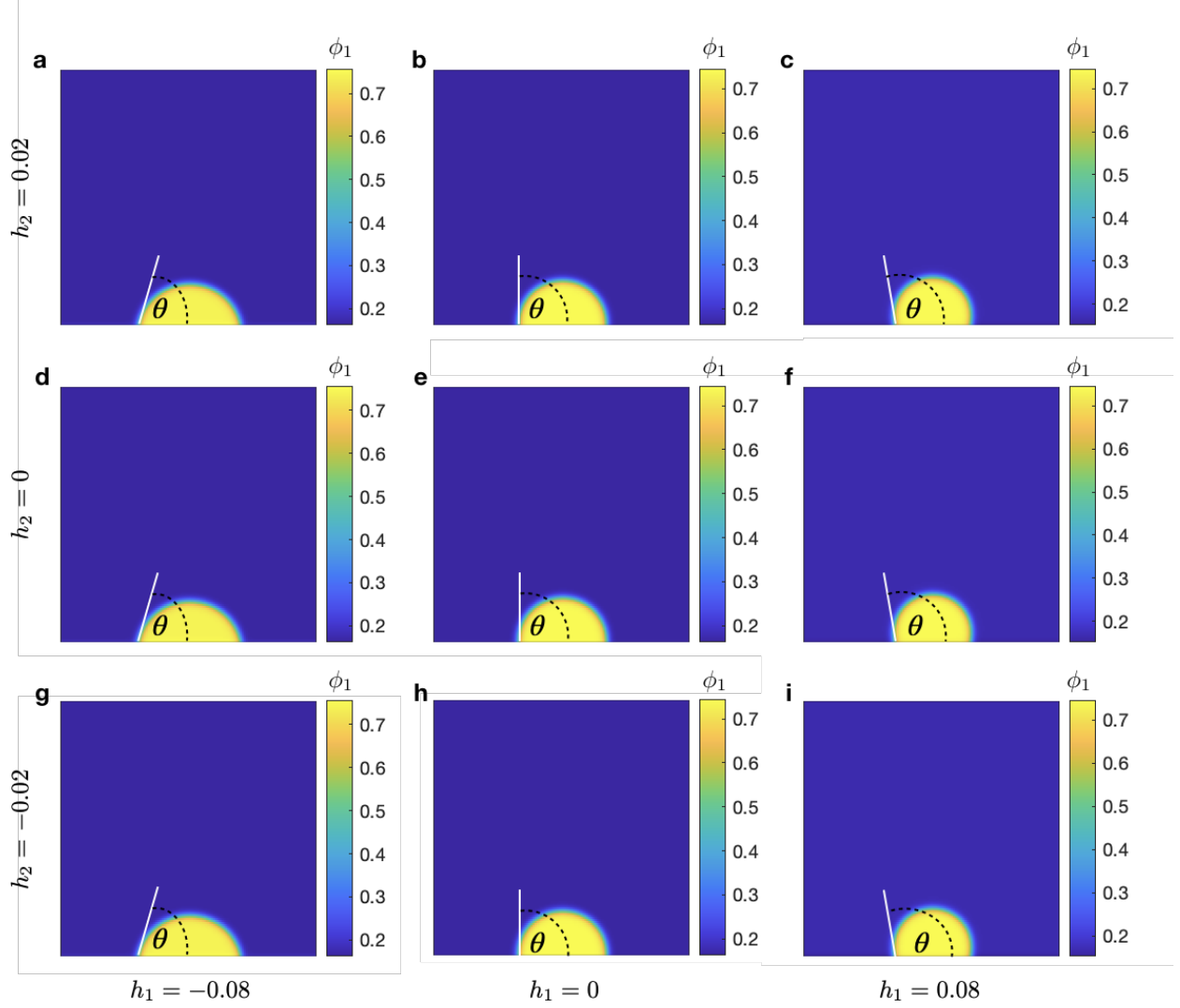


FIG. 2: Profiles of ϕ_1 with a linear interaction between solid walls and mixture components on the contact angle of a two-phase coexisting mixture in equilibrium. The snapshots denote the profiles of component 1, i.e. ϕ_1 with different values of h_1 and h_2 . At each snapshot, the yellow area depicts the condensates, a white line is used to denote the tangent line of the spherical interface at contact point on the surface Γ . The contact angle of droplet between tangent line and surface is denoted by θ . In each column (row), we use same $h_1(h_2)$ values. The basic parameter values used in this case are: $\kappa_{1\Gamma} = \kappa_{2\Gamma} = 0$, $\kappa_1 = \kappa_2 = 1$, $g_1 = g_2 = \gamma = 0$, $\chi_{12} = -1$, $\chi_{23} = 0$, $\chi_{13} = 2.5$. Since the droplet is composite of ϕ_1 mainly, the contact angle is determined by the value of h_1 in this study.

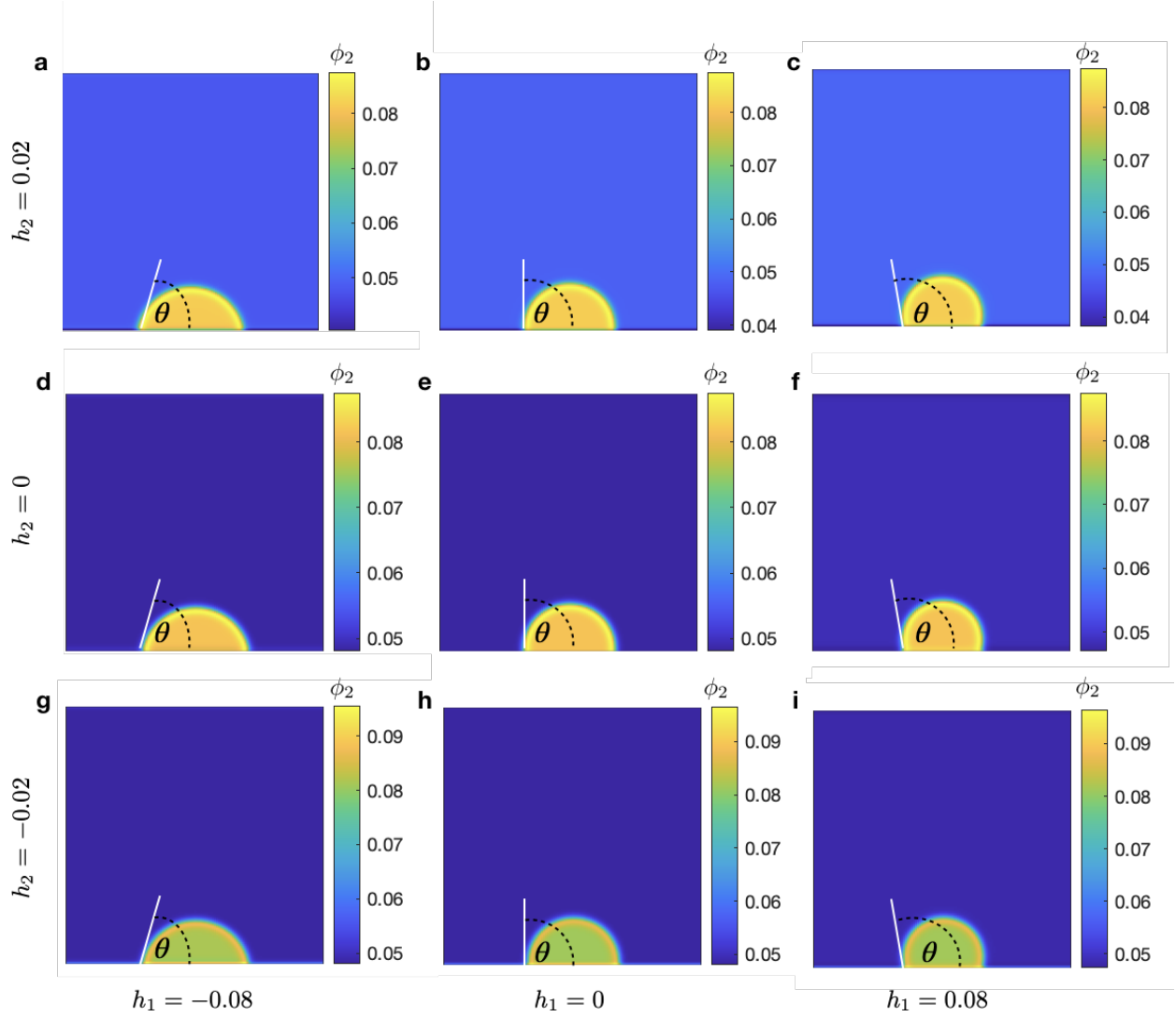


FIG. 3: Profiles of ϕ_2 with a linear interaction between solid walls and mixture components on the contact angle of a two-phase coexisting mixture in equilibrium. The snapshots denote the profiles of component 2, i.e. ϕ_2 with different values of h_1 and h_2 . The profile of ϕ_2 changes rapidly near by the surface with respect to different h_2 values. However, the contact angle is determined by the value of h_1 since the droplet mainly contains ϕ_1 . The basic parameter values used in this case are: $\kappa_{1\Gamma} = \kappa_{2\Gamma} = 0$, $\kappa_1 = \kappa_2 = 1$, $g_1 = g_2 = \gamma = 0$, $\chi_{12} = -1$, $\chi_{23} = 0$, $\chi_{13} = 2.5$.

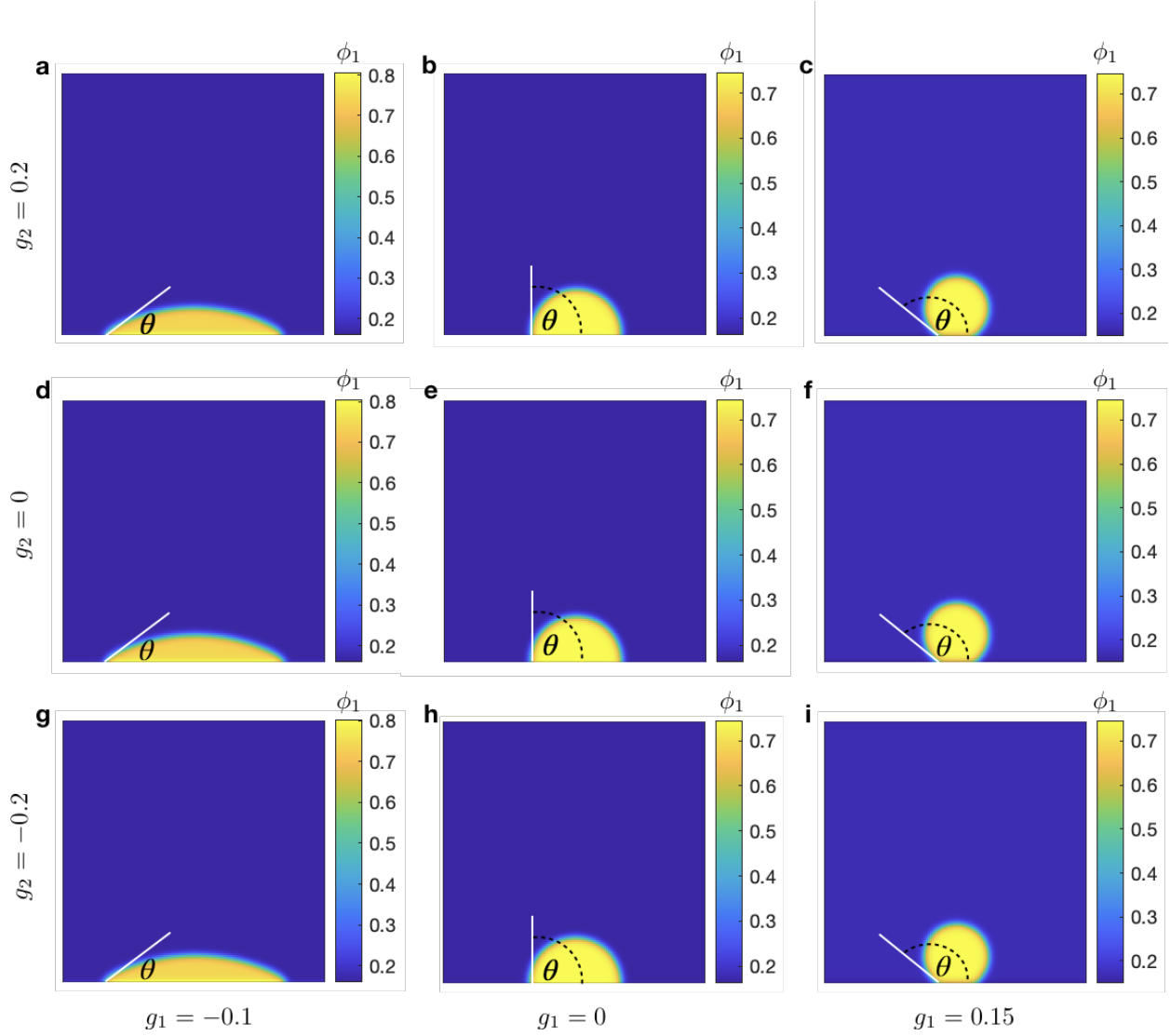


FIG. 4: Profiles of ϕ_1 with a quadratic interaction between solid walls and mixture components on the contact angle of a two-phase coexisting mixture in equilibrium.

The snapshots denote the profiles of component 1, i.e. ϕ_1 with different values of g_1 and g_2 . We observe that the interaction between ϕ_2 and solid wall influences the contact angle mainly. The basic parameter values used in this case are: $\kappa_{1\Gamma} = \kappa_{2\Gamma} = 0$, $\kappa_1 = \kappa_2 = 0$, $h_1 = h_2 = \gamma = 0$, $\chi_{12} = -1$, $\chi_{23} = 0$, $\chi_{13} = 2.5$.

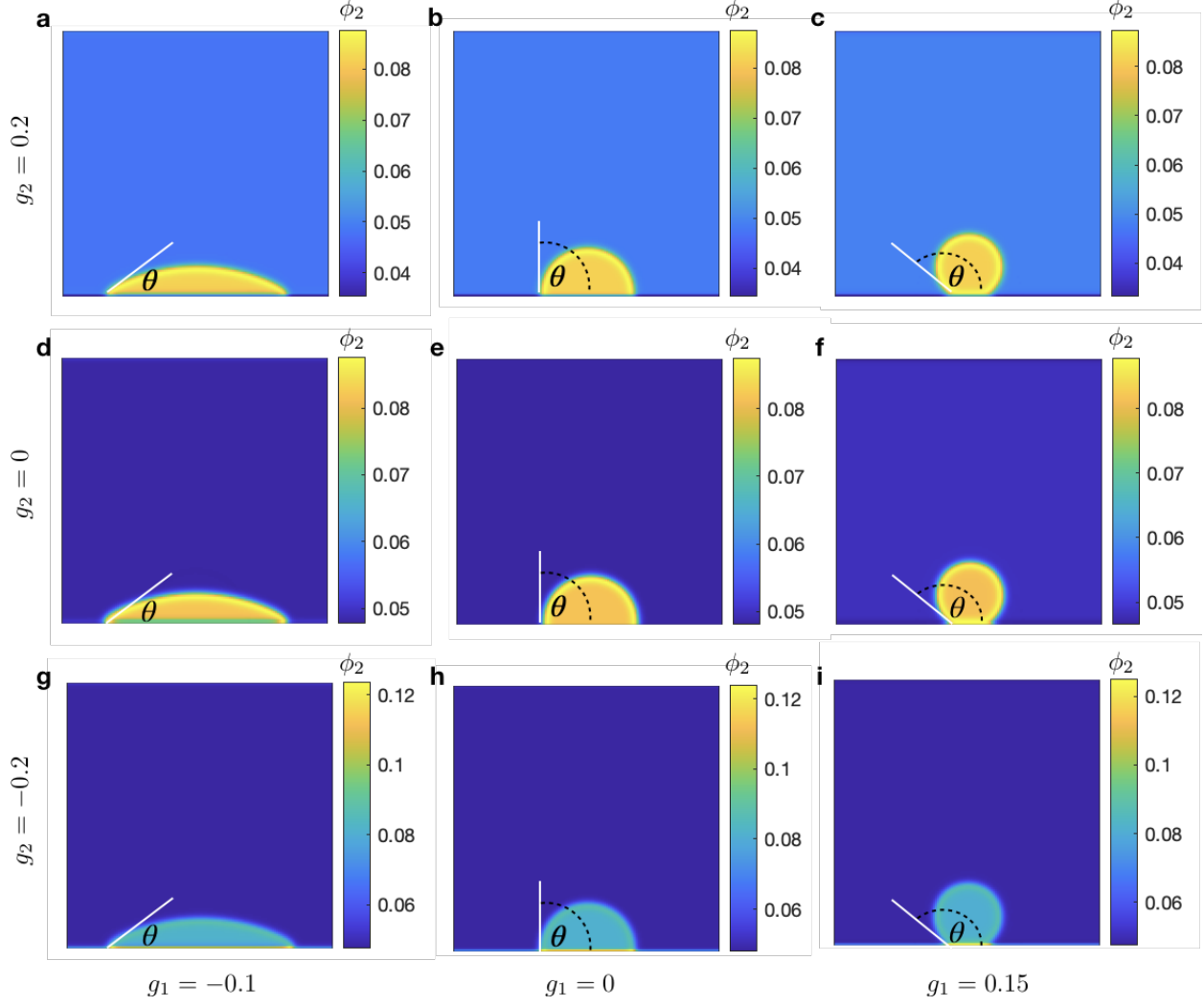


FIG. 5: Profiles of ϕ_2 with a quadratic interaction between solid walls and mixture components on the contact angle of a two-phase coexisting mixture in equilibrium.

The snapshots denote the profiles of component 2, i.e. ϕ_2 with different values of g_1 and g_2 . We find that the interaction between ϕ_1 and solid surface changes the profiles of ϕ_2 near by the surface, while the contact angle is determined by interaction between ϕ_1 and solid wall. The basic parameter values used in this case are: $\kappa_{1\Gamma} = \kappa_{2\Gamma} = 0$, $\kappa_1 = \kappa_2 = 1$, $h_1 = h_2 = \gamma = 0$, $\chi_{12} = -1$, $\chi_{23} = 0$, $\chi_{13} = 2.5$.

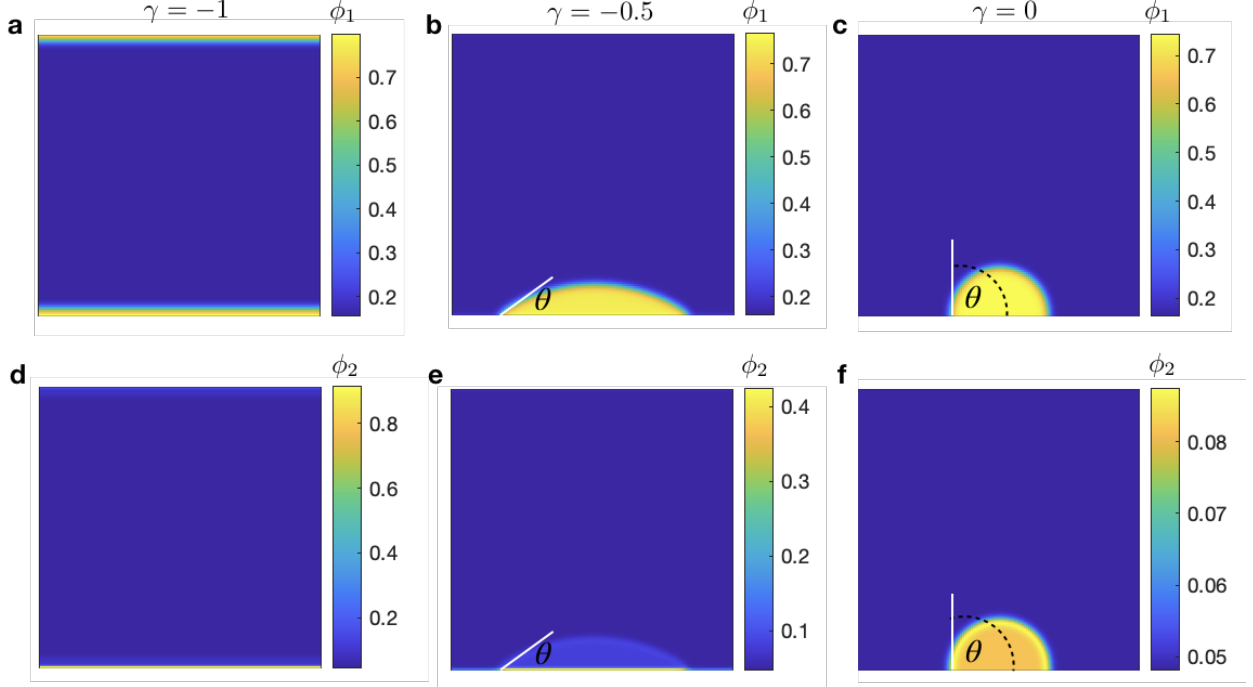


FIG. 6: Profiles of ϕ_1 and ϕ_2 with a nonlinear coupling interaction between ϕ_1 and ϕ_2 in equilibrium. Plots (a, b, c) represent the concentration profiles of ϕ_1 , while plots (d, e, f) the concentration profiles of ϕ_2 . We observe that, as the negative coupling interaction between ϕ_1 and ϕ_2 becomes stronger, the contact angle decreases until the condensate (yellow) completely wets on the solid surface (plots (a, d)). Here, we only investigate the negative coupling interaction, since the positive coupling interaction will lead to nonphysical solutions. The basic parameter values used in this case are: $\kappa_{1\Gamma} = \kappa_{2\Gamma} = 0$, $\kappa_1 = \kappa_2 = 1$, $h_1 = h_2 = g_1 = g_2 = 0$, $\chi_{12} = -1$, $\chi_{23} = 0$, $\chi_{13} = 2.5$.

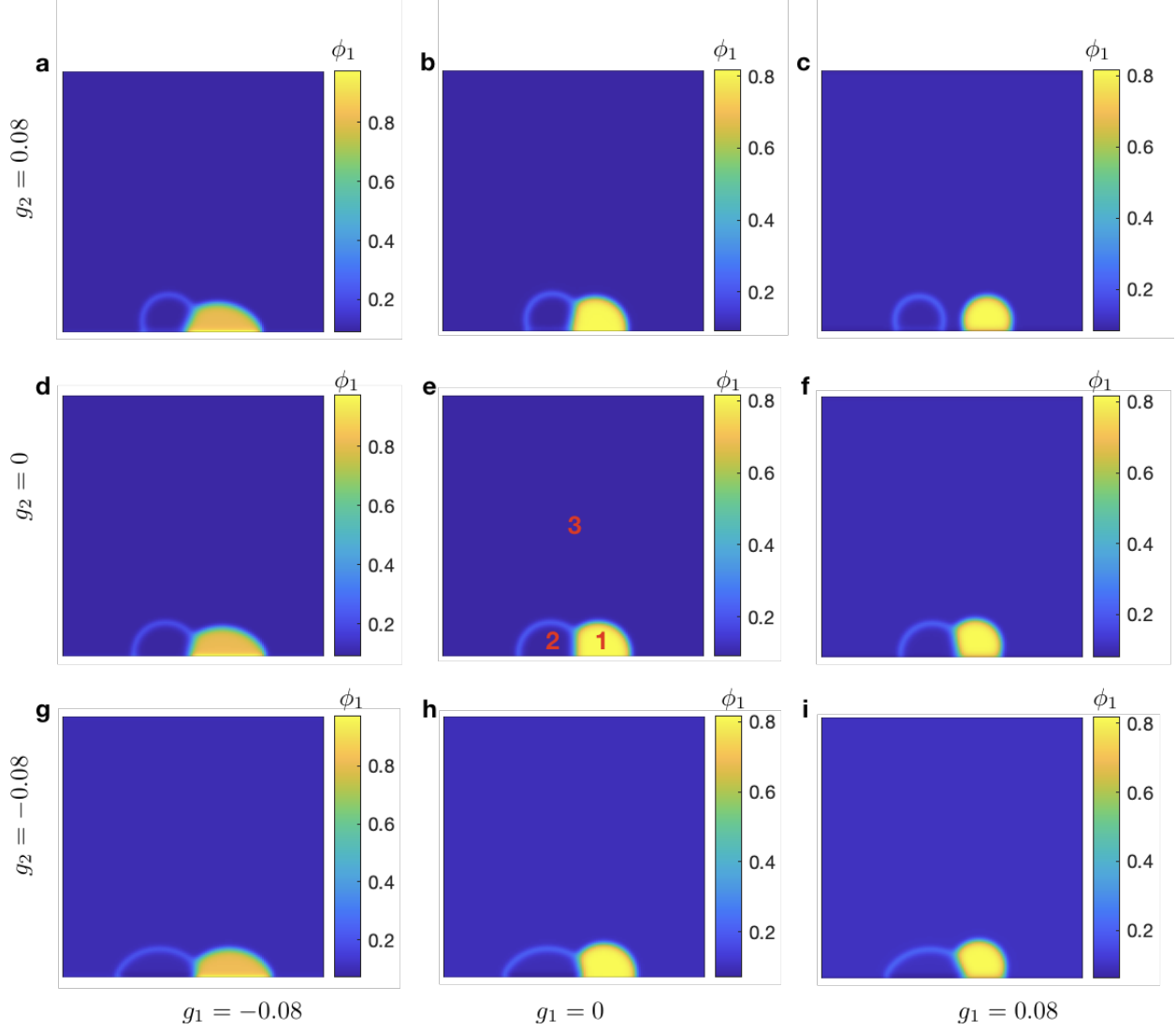


FIG. 7: Profiles of ϕ_1 with a quadratic interaction between solid wall and mixture components on the contact angle of a three-phase coexisting mixture at equilibrium.

With the interaction parameter values $\chi_{12} = \chi_{23} = \chi_{13} = 3$, the ternary mixture has three coexisting phases (denoted by red numbers 1, 2, 3 in plot e). We change the strength of the quadratic interaction, i.e. the values of $g_i, i = 1, 2$. We observe that the contact angle of droplet 1 and 2 are mainly determined by the interaction between the dominant component and the solid wall, i.e. ϕ_1 in droplet 1 and ϕ_2 in droplet 2. Other basic parameter values used in this case are: $\kappa_{1\Gamma} = \kappa_{2\Gamma} = 0$, $\kappa_1 = \kappa_2 = 1$, $h_1 = h_2 = \gamma = 0$.

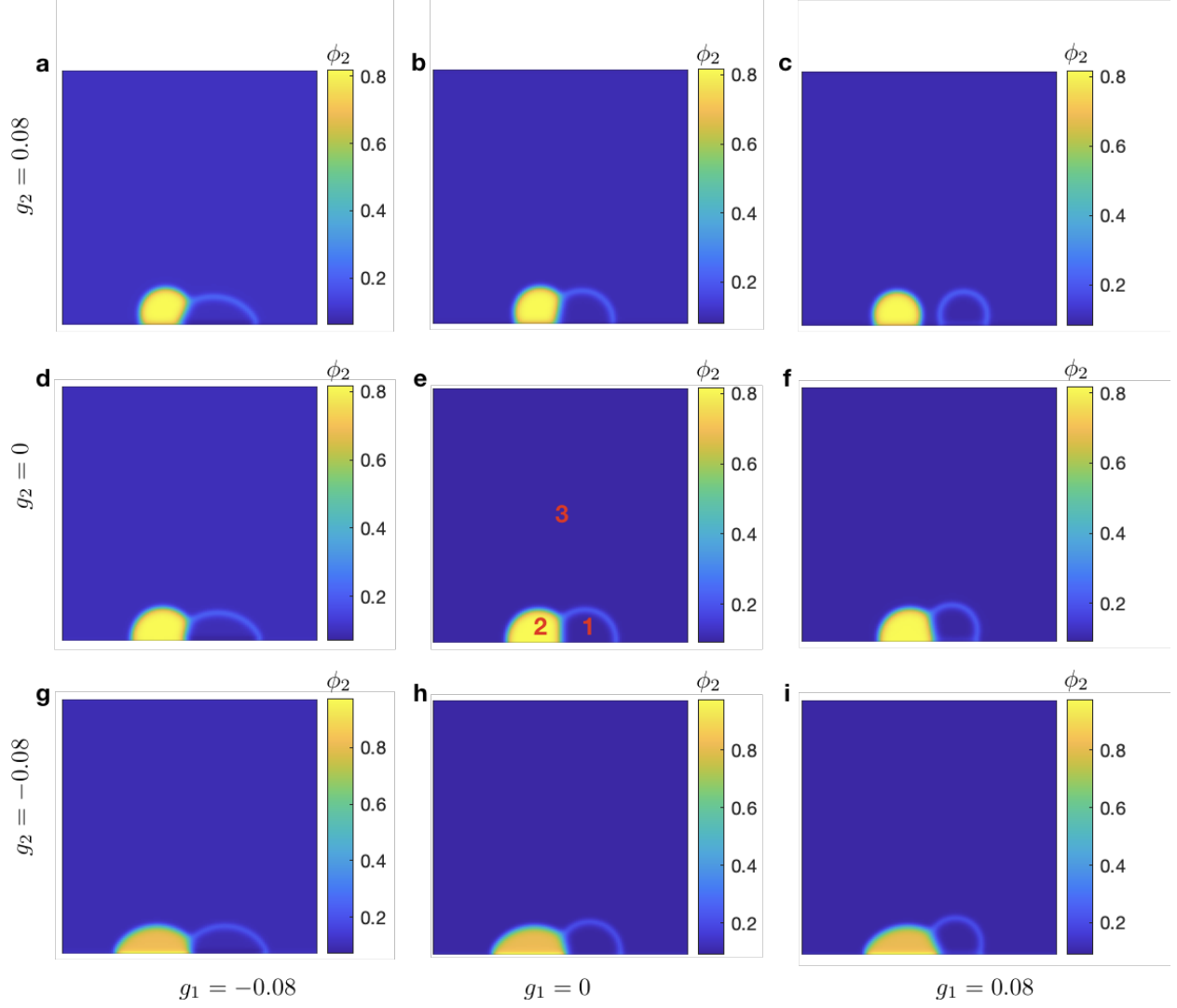


FIG. 8: Profiles of ϕ_1 with a quadratic interaction between solid wall and mixture components on the contact angle of a three-phase coexisting mixture at equilibrium.

The basic parameter values used in this case are: $\kappa_{1\Gamma} = \kappa_{2\Gamma} = 0$, $\kappa_1 = \kappa_2 = 1$, $h_1 = h_2 = \gamma = 0$, $\chi_{12} = \chi_{23} = \chi_{13} = 3$.

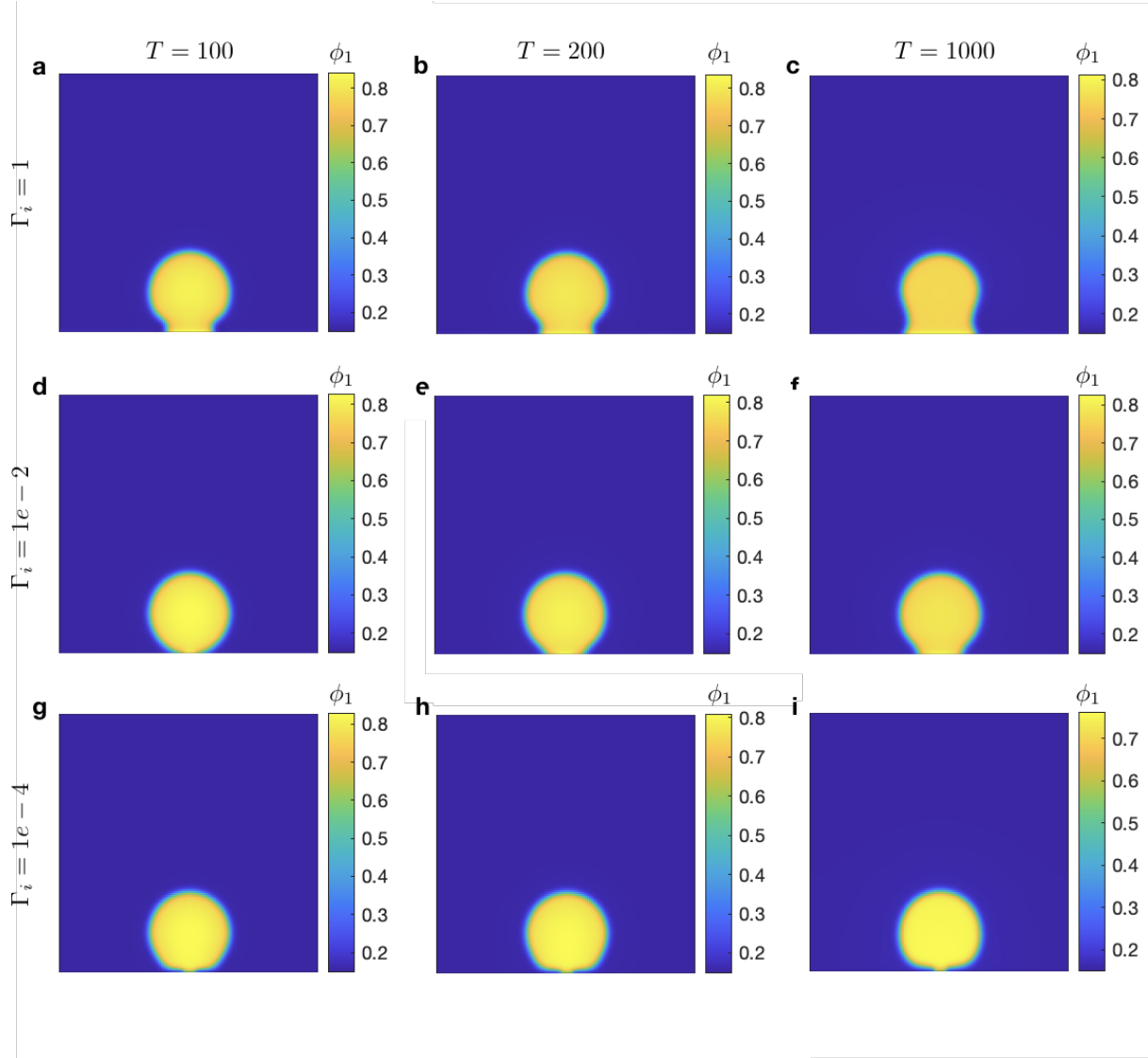


FIG. 9: **Relaxation of dynamic boundary conditions controls the droplet spreading on the surface.** Plots (a-i) are the snapshots of component 1, i.e. ϕ_1 . We do not consider the cross-coupling interaction in this study, i.e. $\Gamma_{12} = 0$. The relaxation rate $\Gamma_i, i = 1, 2$ decrease from 1 to 10^{-4} , the spreading process slows down correspondingly. Other basic parameter values used in this case are: $\kappa_{1\Gamma} = \kappa_{2\Gamma} = 0$, $\kappa_1 = \kappa_2 = 1$, $h_1 = 0, h_2 = 0, g_1 = -1, g_2 = 0, \gamma = 0$, $\chi_{12} = -1$, $\chi_{23} = 0$, $\chi_{13} = 2.5$.

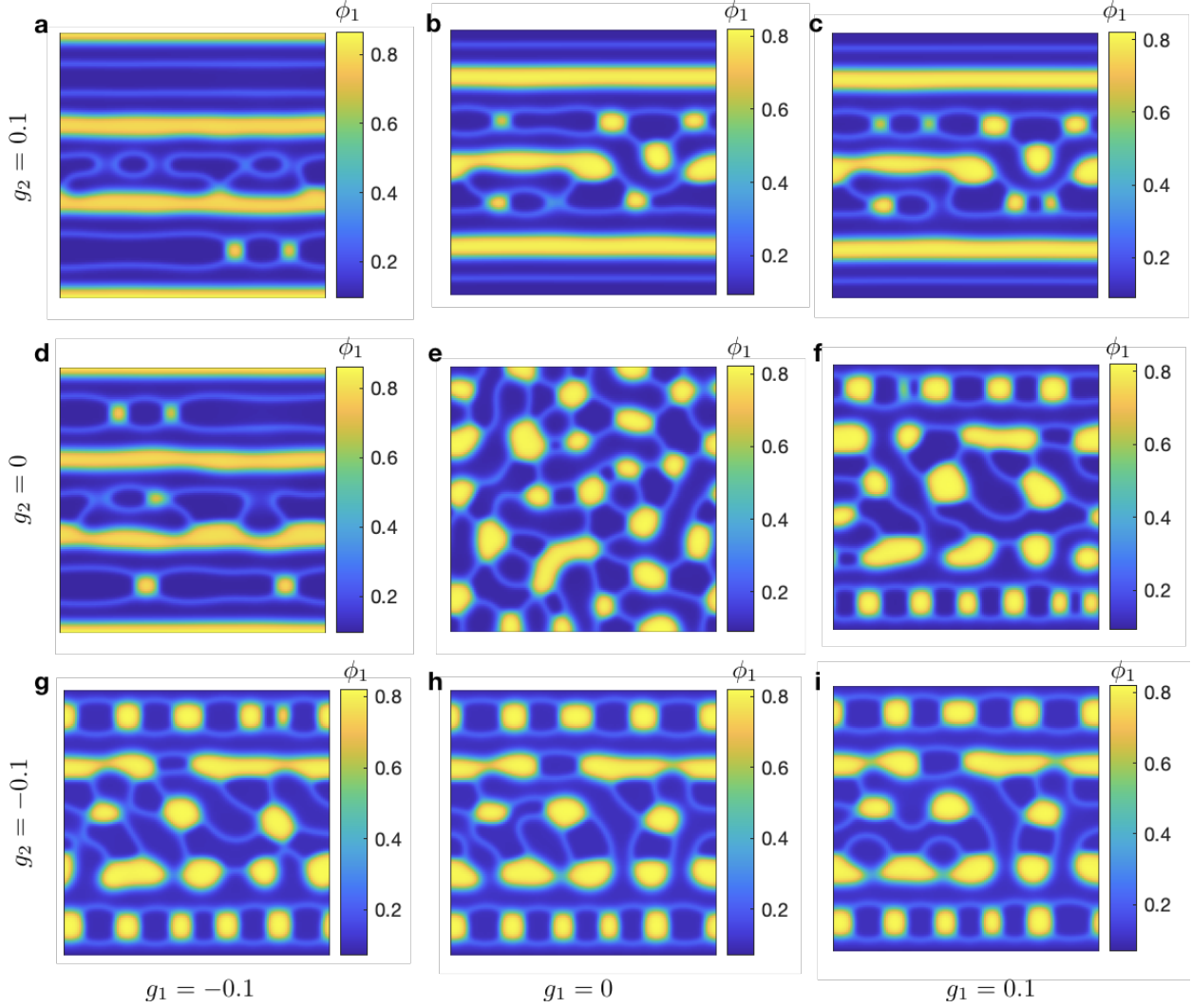


FIG. 10: Profiles of ϕ_1 during the spontaneous phase separation of ternary mixture with three-phase coexistence with various types of wall-mixture interactions. We show the snapshots of ϕ_1 at $T = 10000$. With neutral wall-mixture interaction (plot e, i.e. $g_i = 0, i = 1, 2$), the condensates (yellow) distribute in the bulk homogeneously. However, with attractive/repulsive wall-mixture interaction, the condensates distribute horizontally parallel with the solid wall (see plot a, b, c, d, f, g, i). The basic parameter values used in this case are: $h_1 = h_2 = 0, \kappa_{1\Gamma} = \kappa_{2\Gamma} = 1, \kappa_1 = \kappa_2 = 1, \gamma = 0, \chi_{12} = \chi_{23} = \chi_{13} = 3$.

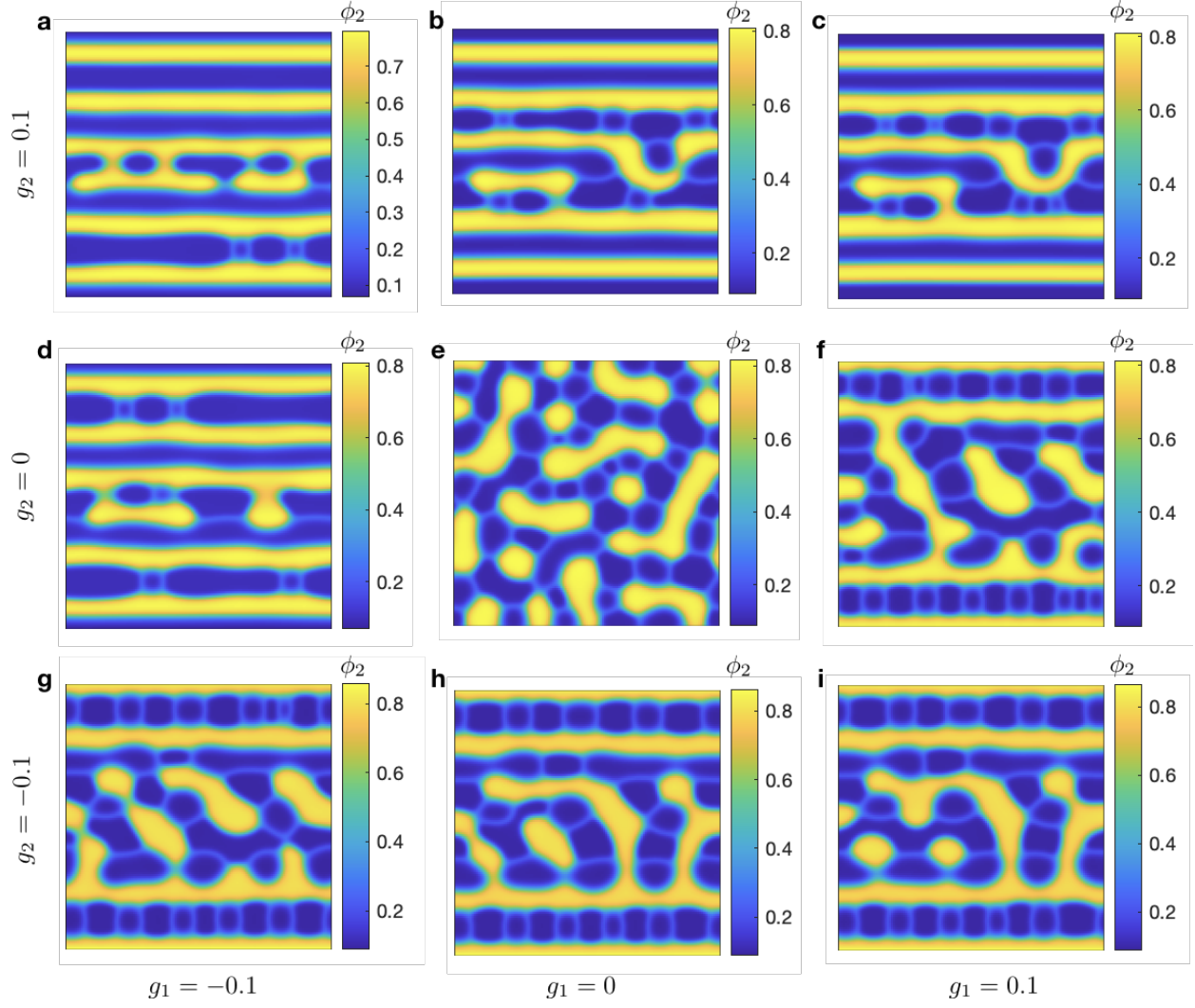


FIG. 11: Profiles of ϕ_2 during the spontaneous phase separation of ternary mixture with three-phase coexistence with various types of wall-mixture interactions. The basic parameter values used in this case are: $h_1 = h_2 = 0$, $\kappa_{1\Gamma} = \kappa_{2\Gamma} = 1$, $\kappa_1 = \kappa_2 = 1$, $\gamma = 0$, $\chi_{12} = \chi_{23} = \chi_{13} = 3$.

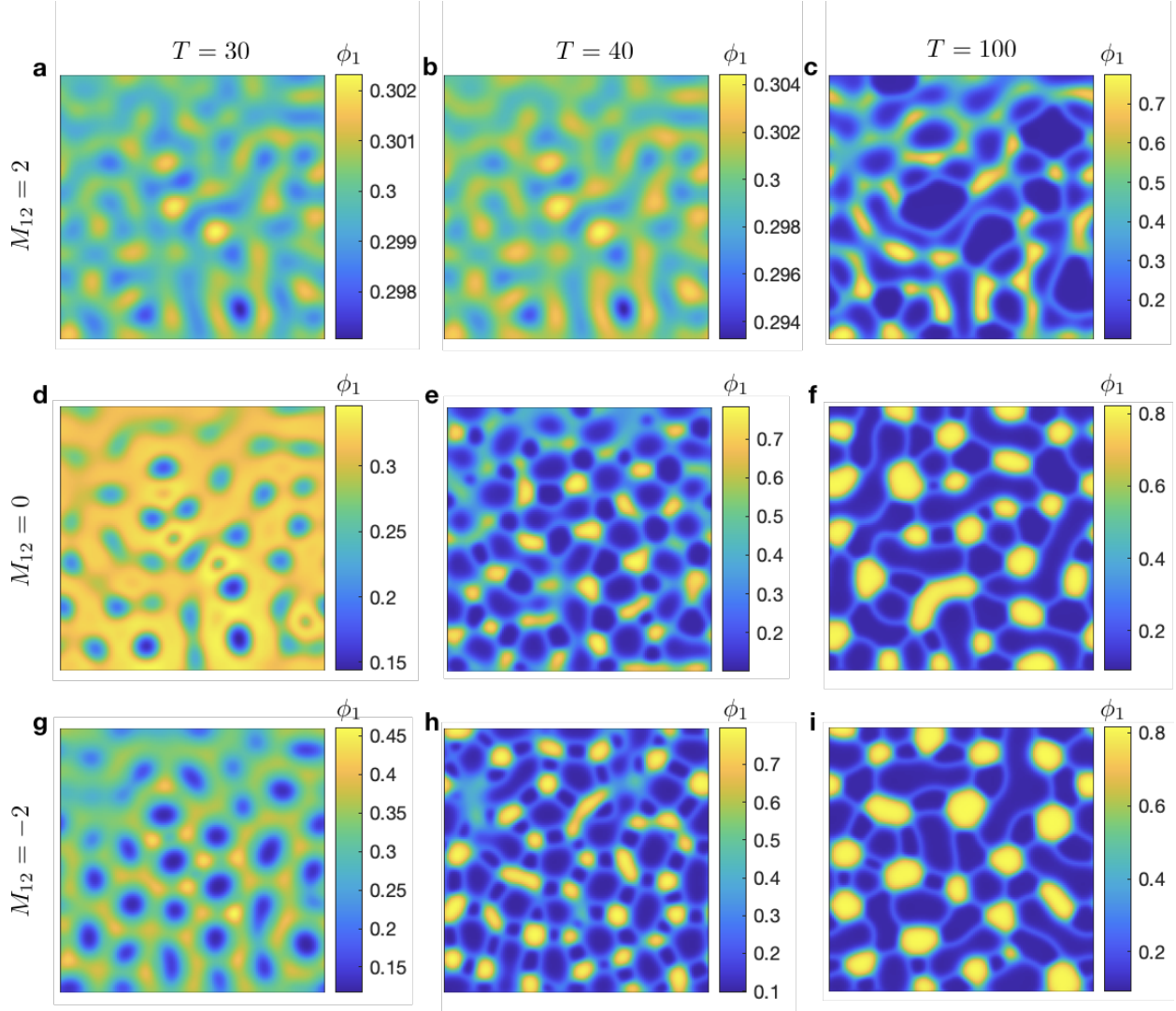


FIG. 12: Profiles of ϕ_1 during spontaneous phase separation evolution at different time points with different values of cross coupling coefficient M_{12} . We find that changing the cross-coupling coefficient M_{12} leads to changes in the phase separation and following coarsening processes. The basic parameter values used in this study are:

$$h_1 = h_2 = g_1 = g_2 = \gamma = 0, \kappa_{1\Gamma} = \kappa_{2\Gamma} = 1, \kappa_1 = \kappa_2 = 1, \gamma = 0, \chi_{12} = \chi_{23} = \chi_{13} = 3.$$

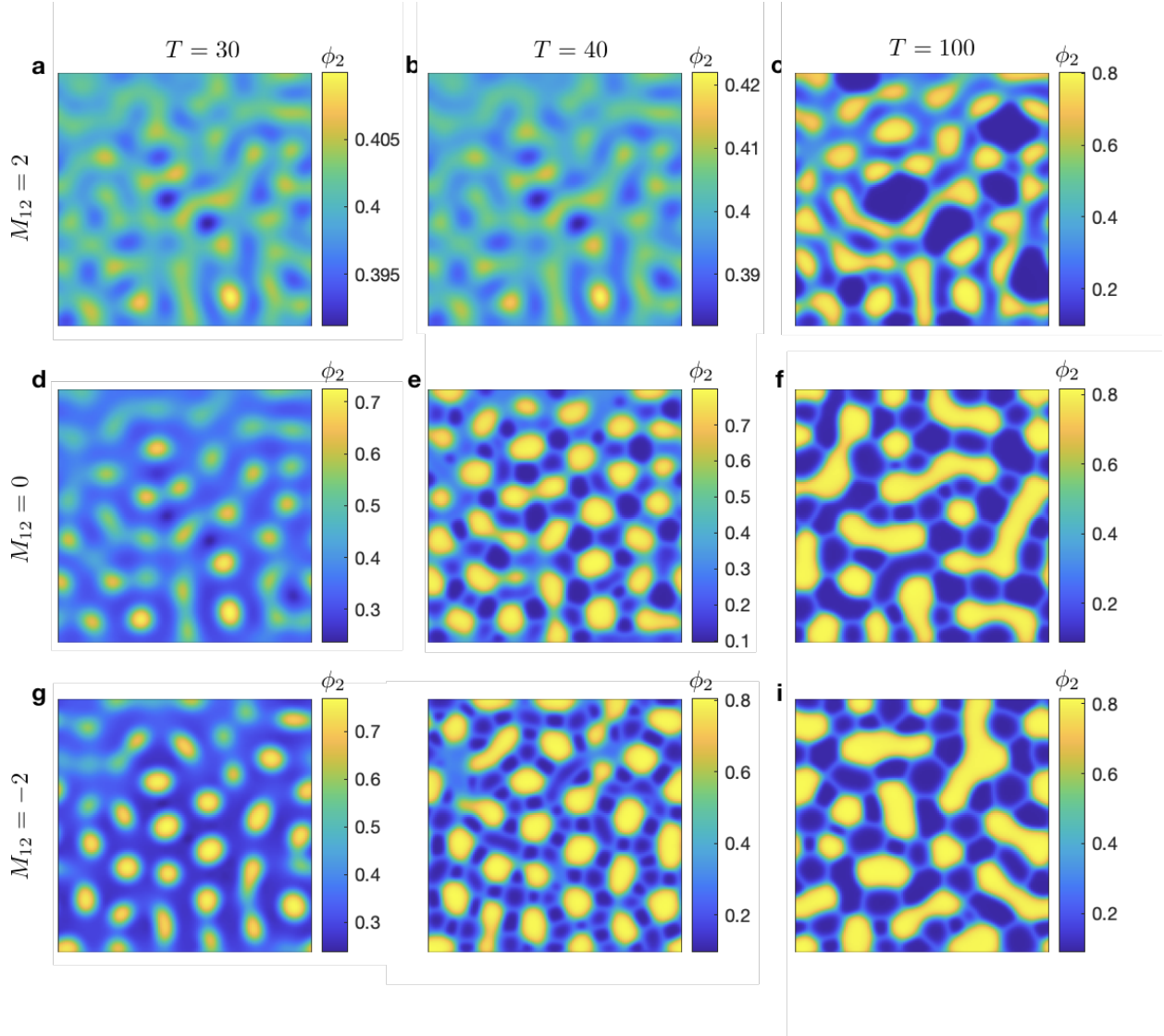


FIG. 13: Profiles of ϕ_2 during spontaneous phase separation evolution at different time points with different values of cross-coupling coefficient M_{12} . The basic parameter values used in this case are: $h_1 = h_1 = g_1 = g_2 = \gamma = 0$, $\kappa_{1\Gamma} = \kappa_{2\Gamma} = 1$, $\kappa_1 = \kappa_2 = 1$, $\gamma = 0$, $\chi_{12} = \chi_{23} = \chi_{13} = 3$.

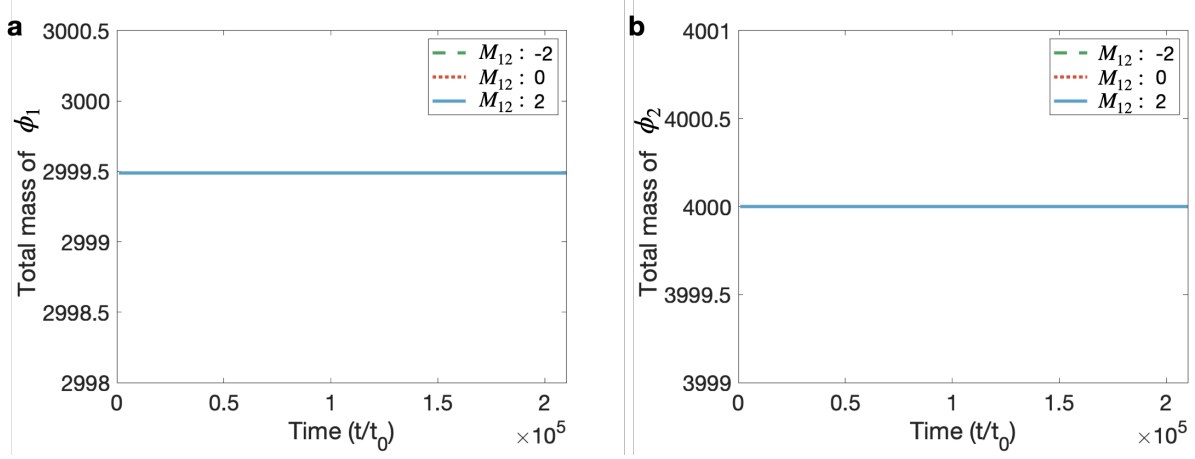


FIG. 14: **Total mass of ϕ_1 and ϕ_2 in the system during spontaneous phase separation**

process. The basic parameter values used in this case are: $h_1 = h_1 = g_1 = g_2 = \gamma = 0$,

$\kappa_{1\Gamma} = \kappa_{2\Gamma} = 1$, $\kappa_1 = \kappa_2 = 1$, $\gamma = 0$, $\chi_{12} = \chi_{23} = \chi_{13} = 3$.

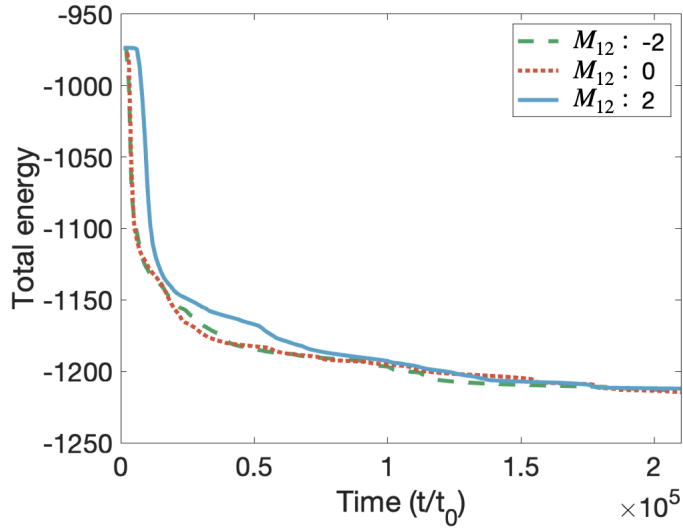


FIG. 15: **Total energy profiles during spontaneous phase separation process with**

different cross-coupling coefficient M_{12} . The basic parameter values used in this case are:

$h_1 = h_1 = g_1 = g_2 = \gamma = 0$, $\kappa_{1\Gamma} = \kappa_{2\Gamma} = 1$, $\kappa_1 = \kappa_2 = 1$, $\gamma = 0$, $\chi_{12} = \chi_{23} = \chi_{13} = 3$.

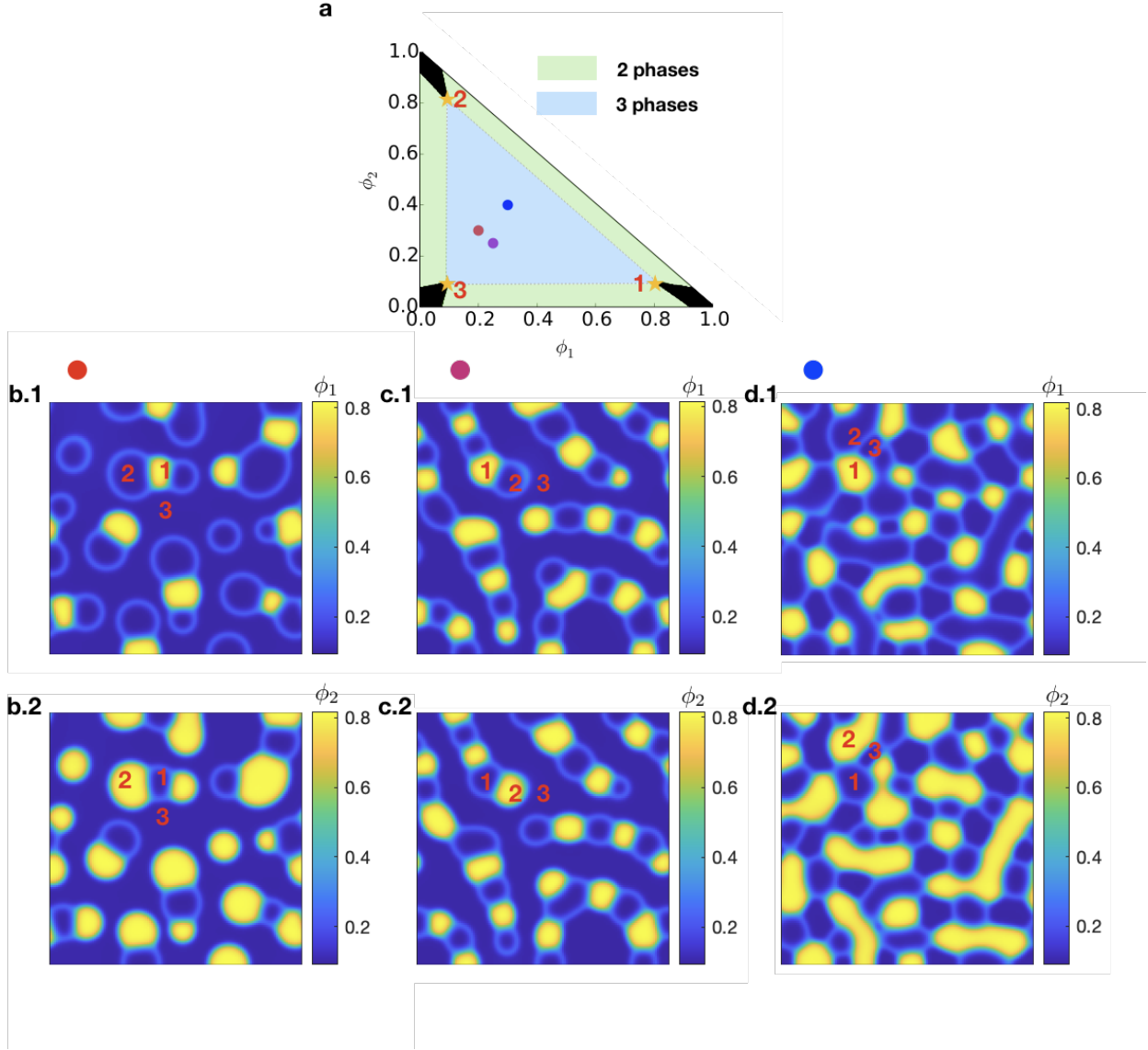


FIG. 16: Phase diagram of ternary mixture and three-phase coexistence examples. Plot **a** is the phase diagram of ternary mixture. Black region depicts the case with one homogeneous phase; Green region depicts the case with two phases; Blue region denotes the case with three coexisting phases. Plots **b.1-b.2**, **c.1-c.2**, **d.1-d.2** are snapshots of ϕ_1 and ϕ_2 with different sets of the initial composition, which are marked by the color dots in the blue region. The basic parameter values used in this case are: $h_1 = 0, h_2 = 0, \kappa_1 = \kappa_2 = 1, g_1 = g_2 = \gamma = 0, \chi_{12} = \chi_{23} = \chi_{13} = 3$.

TABLE II: Notations

Notations	Explanations
χ_{ij}	interaction strength between the component i and j
γ	coupling interaction strength between components on the surface
Γ	boundary of domain
Γ_i	relaxation parameters of dynamic boundary condition, i=1,2,12
κ_B	Boltzmann constant
$\kappa_i, \kappa_{i\Gamma}$	gradient coefficients associated with interface free energies, i=1,2,12
μ_i	chemical potentials in the bulk for components i=1,2
$\mu_{i\Gamma}$	chemical potentials on the surface for components i=1,2
Δ_Γ	Laplace–Beltrami operator on the boundary surface
ν_i	molecule volume of component i, i=1,2
Ω	domain
ω_i	internal free energy coefficient for component i in the bulk
ϕ_i	volume fractions of three components, i=1,2,3
$\phi_{i\Gamma}$	volume fractions of component, i=1,2
D_i	diffusion coefficients, i=1, 2, 12.
f_b	bulk free energy density function
f_s	surface free energy density function
g_i	molecule-molecule interaction strength of each components near by the wall
h_i	interaction strength proportional to the component volume fractions, i=1, 2.
M_i	mobility, i=1, 2, 12.
T	temperature of the isotropic system